AD-A186 889 FABRICATION AND PACKAGING OF DISCONTINUOUS MIM (METAL-INSULATOR-METAL) FI (U) NORTH CAROLINA AGRICULTURAL AND TECHNICAL STATE UNIV GREENSBO

1/1

UNCLASSIFIED Y CHUNG OCT 87 ARO-20731 4-EL-H F/G 9/1 NL

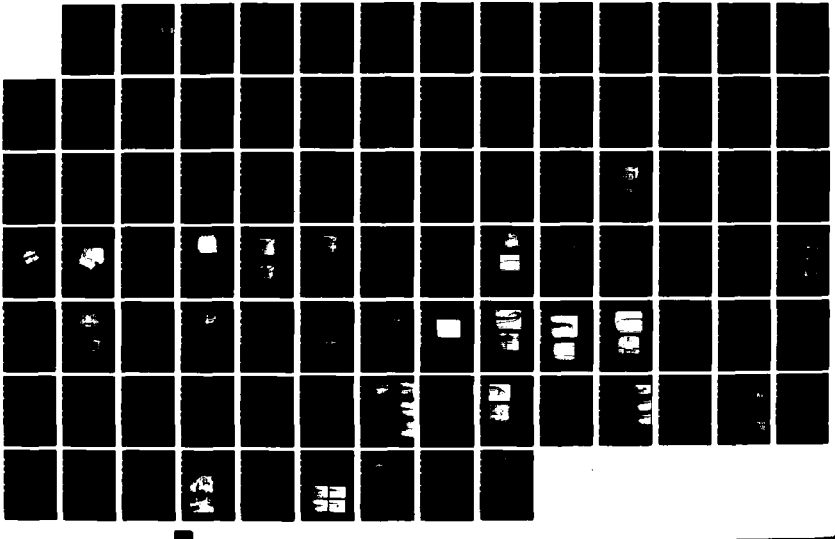

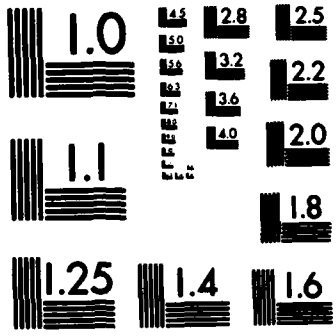

MICROCOPY RESOLUTION TEST CHART
NATIONAL BUREAU OF STANDARDS-1963-A

ARO 20731.4-EL-H

FABRICATION AND PACKAGING OF DISCONTINUOUS MIM FILM ARRAYS FOR EFFICIENT MM WAVE AND IR DETECTION AND MIXING

FINAL REPORT

GRANT NO. DAAG 29-83-G-0114

PERIOD: September 5, 1983 - August 12, 1987

ARMY RESEARCH OFFICE

RESEARCH TRIANGLE PARK

NORTH CROLINA

SUBMITTED BY

DR. CHUNG YU

ELECTRICAL ENGINEERING DEPARTMENT

NORTH CROLINA A & T STATE UNIVERSITY

GREENSBORO, NC 27411

A186 809

SECURITY CLASSIFICATION OF THIS PAGE (When Data Entered)

REPORT DOCUMENTATION PAGE		READ INSTRUCTIONS BEFORE COMPLETING FORM
1. REPORT NUMBER ARO 20731.4-EL-H	2. GOVT ACCESSION NO.	3. RECIPIENT'S CATALOG NUMBER
4. TITLE (and Subtitle) FABRICATION AND PACKAGING OF DISCONTINUOUS MIM FILM ARRAYS FOR EFFICIENT MM WAVE AND IR DETECTION AND MIXING		5. TYPE OF REPORT & PERIOD COVERED Final Technical Report; 9/5/83 - 8/12/87 6. PERFORMING ORG. REPORT NUMBER
7. AUTHOR(s) Chung Yu		8. CONTRACT OR GRANT NUMBER(s) DAAG 29-83-G-0114
9. PERFORMING ORGANIZATION NAME AND ADDRESS North Carolina A & T State University, Greensboro, NC 27411		10. PROGRAM ELEMENT, PROJECT, TASK AREA & WORK UNIT NUMBERS P-20731-EL-H
11. CONTROLLING OFFICE NAME AND ADDRESS U. S. Army Research Office Post Office Box 12211 Research Triangle Park, NC 27709		12. REPORT DATE October, 1987 13. NUMBER OF PAGES 61
14. MONITORING AGENCY NAME & ADDRESS(if different from Controlling Office) Department of the Navy, Office of Naval Research, George Institute of Gechnology, 206 O'Keefe Bldg., Atlanta, GA 30332-0490		15. SECURITY CLASS. (of this report) 15a. DECLASSIFICATION/DOWNGRADING SCHEDULE

16. DISTRIBUTION STATEMENT (of this Report)

Approved for public release; distribution unlimited.

17. DISTRIBUTION STATEMENT (of the abstract entered in Block 20, if different from Report)

NA

18. SUPPLEMENTARY NOTES

THE VIEW, OPINIONS, AND/OR FINDINGS CONTAINED IN THIS REPORT ARE THOSE OF THE AUTHOR(S) AND SHOULD NOT BE CONSTRUED AS AN OFFICIAL DEPARTMENT OF THE ARMY POSITION, POLICY, OR DECISION, UNLESS SO DESIGNATED BY OTHER DOCUMENTATION.

19. KEY WORDS (Continue on reverse side if necessary and identify by block number)

MIM array; Whisker tip enhancement and stabilization; Tunneling conduction mechanisms

20. ABSTRACT (Continue on reverse side if necessary and identify by block number)

Sputtering desposition of discontinuous Ni islands on a glass plate automatically produces a planar MOM diode array structure that will be mechanically stable when electrical leads are silver soldered to any two points of the coated plate. However, the efficiency in radiation reception and detection is totally controlled by the geometry of the diode array or the deposition process, which is mostly random due to deposition at very low sputtering powers. Such an array structure also has very poor antenna —

DD FORM 1 JAN 73 1473 EDITION OF 1 NOV 65 IS OBSOLETE

SECURITY CLASSIFICATION OF THIS PAGE (When Data Entered)

properties.

Diode responsivity is found to be significantly improved by the incorporation of an etched-tip tungsten whisker, serving both as a long wire antenna for radiation reception and as a sharp tip electrical contact that concentrates the incident field and directs it to a selected nickel island group. This improvement in diode responsivity is offset by degradation in diode stability similar to that experienced by the MOM point contact diode, but to a lesser extent. The distinction between these two structures lies in the fact that the whisker serves mainly as an electrical contact in the discontinuous film diode, while it serves as the other electrode, sandwiching an ultrathin oxide layer, in the point contact version. Stability can again be improved by deliberate hooking of an optimally etched tip without blunting. Some blunting is acceptable in the film diode at the expense of reduced diode responsivity.

To further improve stability against major mechanical shocks, the whisker stem is bent by design and the entire whisker cemented to a glass plate, which is then glued onto a second plate coated with the discontinuous nickel film. This assembling technique causes the etched tip of the whisker to make contact with the nickel coated plate and be hooked in the process. A proper mounted diode assembly is highly stable when pacakged in microwave waveguide, on which provision is made for IR radiation access.

To further understand the conduction mechanism in these diodes, a program has been initiated to study the fundamental conduction mechanisms proposed by many researchers, but hitherto untested experimentally due to the dominance of instabilities inherent in most of the MOM diodes reported. The single-junction point contact diode will serve as the basic model. The mechanisms of interest are thermally assisted tunneling, plasmon conduction, tunnel junction modes and irradic switching.

The removal of thermal instabilities has enabled us to study thermally assisted tunneling and its effect on diode conduction. Since plasmon conduction is dependent on the shape of the antenna, control of the etched whisker tip will lead to control of the plasmon conduction process. The control and definition of the geometry of the tunneling junction region will determine tunnel junction modes and their efficient coupling. The junction geometry also affects fundamentally the switching phenomenon and hence diode noise properties. This is the first time a highly stabilized MOM diode has been fabricated that can have the potential of verifying these theoretical models.

PUBLICATIONS RESULTING FROM THE GRANT

1. C. Yu, and A. Niczad, "Field Enhancement and Increased Island Array Selectivity of the Discontinuous MIM Film Diode", Proc. 10th Intern. Conf. On Infrared and MM Waves, Lake Buena Vista, Florida (Dec. 1985), p. 135.

2. C. Yu, M. Hemmatian, and A. Yekrangian, "Mounting Improvements of the MOM Point Contact Diode", Proc. 10th Intern. Conf. on Infrared and MM Waves, Lake Buena Vista, Florida (Dec. 1985) p. 133.

3. C. Yu, M. A. Hemmatian, A. Niczad, Y. Taghipoor, and A.Yekrangian, "A Systematic Study of the Effect of Hooking Upon Contact on the Performanc of Electrolytically Etched Point Contact MOM Diodes", Proc. SPIE 544, 78 (1985).

4. C. Yu, and A. Sabzali, "Guided Transmission for 10 μm Tunable Lasers", Proc. SPIE 717, 33 (1986).

5. C. Yu, and C. K. Fong, "Investigation of Stimulated Brillouin Scattering Switching in Mid IR Fibers", Proc. SPIE's O-E/Fibers'87, Symp. on Fiber Optics and Integrated Optoelectronics, San Diego, CA (Aug. 16-21, 1987).

6. C. Yu, and C. S. Tan, "Responsivity and Noise Properties of a Highly Stabilized MOM Point Contact Diode for High Power Mid IR Detection and Mixing", Accepted for presentation at the 10th Intern. Conf. on Lasers'87, Lake Tahoe, Nevada (Dec. 7-11, 1987).

7. C. Yu, and C. K. Fong, "Study of Nonlinear Optical Phenomena in Mid IR Fibers",, Accepted for presentation at the 10th Intern. Conf. on Lasers'87, Lake Tahoe, Nevada (Dec. 7-11, 1987).

8. C. Yu, C. K. Fong, and C. S. Tan, "Phonon Probe for Laser Propagation Studies in Mid IR Fibers", accepted for presentation at the 12th Intern. Conf. on Infrared and MM Waves, Orlando, Florida (Dec. 14-18, 1987).

SCIENTIFIC PERSONNEL SUPPORTED DIRECTLY OR INDIRECTLY BY THE GRANT

1. A. Niczad - MSEE degree (1986);
2. M. A. Hemmatian - MSEE program in progress;
3. A. Yekrangian - MSEE degree (1986);
4. C. K. Fong - MSEE degree expected 1987;
5. C. S. Tan - MSEE degree expected 1987;
6. A. Sabzali - MSEE degree (1987);
7. F. Flores - MSEE degree expected 1988.

TABLE OF CONTENTS

LIST OF TABLES. . . . . .

LIST OF ILLUSTRATIONS. . . . . .

CHAPTER PAGE

I INTRODUCTION. . . . . .

1.1 Metal-Insulator-Metal diodes 1
1.2 Characteristic features of the MIM film diode 2

II ANALYSIS OF MIM FILM DIODE OPERATION. . . . . .

2.1 Theory of the catswhisker antenna property 5
2.2 Tunnel-effect in the MIM (Metal-Insulator Metal) structure. 10

III DISCONTINUOUS MIM FILM DIODE STRUCTURE. . . . . .

3.1 MOM diode background technology 20
3.2 Alternative structure of MIM film diode 24
3.3 Film characteristics 26
3.4 Film deposition 28
3.5 Electrolytic etching of the catswhisker 30
3.6 Catswhisker tip contacting or hooking process 30
3.7 Diode packaging 30

IV TEST RESULTS ON MIM FILM DIODE. . . . . .

4.1 Film selection 35
4.2 Selection of etched tungsten whisker 40
4.3 X-band detection of MIM film diode 44

V CONCLUSION. 58

REFERENCES 59

APPENDIX

LIST OF ILLUSTRATIONS

FIGURE	
1.1	Region of island size and separation at which the proposed conduction mechanisms are most applicable
2.1	Shape of etched tips for different immersion depths after contact is made
2.2	The tip of the etched whisker for different hook formation
2.3	Schematic representation of the tunnel effect (a) for a thick barrier (b) for a very thin barrier
2.4	Potential energy diagram of (a) metal-vacuum interface after Sommerfeld, and (b) metal-vacuum-metal interface
2.5	General potential barrier in insulating film between two metal electrodes
2.6	Illustration of Eq. (32) showing current flow between the electrodes
3.1	Conventional point-contact diode structure
3.2	MOM point-contact diode structure
3.3	(a) Single chip with leads (b) Chip arrays in series and parallel
3.4	Sketch of film diode and mount
3.5	SEM pictures of etched tungsten tips (x3000 magnification)
3.6	Cross sectional view of waveguide packaging
3.7	Mounting of the film diode inside the X-band waveguide.
3.8	Waveguide diode packaging
4.1	The I-V curve of five different films (a) I-V curve of (100W, 30 sec) Ni film (b) I-V curve of (100W, 15 sec) Ni film (c) I-V curve of (50W, 45 sec) Ni film (d) I-V curve (50W, 30 sec) of Ni film (e) I-V curve (50W, 20 sec) of Ni film

FIGURE

4.2	Photographs of etched tip before and after blunting (using SEM)
4.3	Photographs of etched tip before and after hooking (using SEM)
4.4	Photographs of etched tip before and after hooking (using SEM)
4.5	Microwave setup used for detection and mixing of the waveguide packaging diode
4.6	I-V curve of the Ni film (50W, 30 sec) (R - 9Ω) chips aray and field enhanced MIM film diodes (b) X-band detection of chips array MIM film diode (c) X-band detection of field enhanced film diode
4.7	I-V curve of Ni film and corresponding detected signal (a) (50W, 30 sec) (R = 6K) (b) (50W, 30 sec) (R = 9KΩ) (c) (50W, 30 sec) (R = 14 KΩ) (d) (50W, 30 sec) (R = 1.6KΩ)
4.8	I-V curve of the Ni film and corresponding X-band beat signal of MIM film diode and the commercial diode
4.9	I-V curve of the Ni film used in three different waveguide packaged diode with different cats-whiskers (catswhiskers with different slender ratios)
4.10	SEM photography of a hooked tip and corresponding X-band detection of waveguide packaged MIM film diode
4.11	SEM photograph ofa hooked tip and corresponding X-band detection of waveguide-packaged MIM film diode
4.12	SEM photograph of a blunted tip and corresponding X-band detection of waveguide-packaged MIM film diode

LIST OF TABLES

TABLE

4-1 Resistance range of thin Ni film in five different deposition conditions. . . . . .

CHAPTER I

INTRODUCTION

1.1 Metal-Insulator-Metal Diodes

Radiation detection in the wavelength range from mm to the infrared can used both microwave and infrared technqiues. A traditional infrared technique, photodetectors, is often used for both detection and mixing. Photodetectors, however are much slower than interactive detectors. They also require refrigeration, especially in the far infrared. Vacuum tubediodes are not usable at submillimeter wavelength, as they suffer from "transit time effect". Alternatively, one may use traditional nonlinear room temperature diodes, such as point-contact diodes or metal-semiconductor schottky barrier diodes. The use of point-contact diodes as detectors in the submillimeter region has some advantages over other infrared detectors, since it has low junction capacitance, hence an inherently fast response.

The earliest point-contact Metal-Insulator-Metal (MIM) device reported in the literature utilized a catswhisker tungsten wire in contact with a polished metal plate [6]. The contact was not ohmic due to some trapped materials (i.e., oxide) at the contact, and conduction was assumed to occur by means of electrons which tunnel through the

insulator. This particular tunnel configuration had a very small capacitance (10^{-2}PF) and a low spreading resistance, which led to a limiting "RC time constant" of the order of 10^{-13}s [1].

Unfortunately, the extreme mechanical instability of the point-contact MOM configuration made it unusable as a practical device. Many attempts have been made to fabricate a stable, integrated device as an alternative to the MOM point-contact diode. One such diode uses discontinuous nickel films, vacuum deposited onto a glass substrate [2-4]. This diode is a hybrid structure that utilized the planar feature of film deposited on a planar glass plate for stability and reintroduction of the etched whisker tip of the point-contact diode in contact with the island arrays for array selection and local field enhancement [5].

1.2. Characteristic Features of the MIM Film Diode

When metal is vacuum-deposited onto a substrate such as a glass slide, it is clear that the film is discontinuous at the beginning of deposition. Numerous metal islands are formed on the substrate, each of which grows with the adsorption of atoms onto the substrate. Continued deposition of metal atoms finally brings about direct contacts of islands leading to the establishment of a continuous film.

Even when the islands are separated, the discontinuous metal film exhibits electrical conduction. The principal mechanism for conduction is considered to be the passage of electrons through the insulating layers between islands by tunneling [7,8]. In films with high density of small islands, direct tunneling will be the principal conduction

mechanism. On the other hand, as the distance between islands and the sizes of the islands are increased, the conduction process becomes complicated, and may involve conduction via impurity levels of the substrate materials, thermal excitation of electrons in the islands and thermal electron emission. According to Neugebauer, the electrical conduction mechanism is related to the structure of the thin film as shown in Figure 1 [9]. When the film has the discontinuous structure corresponding to region A, where direct tunneling is the dominant conduction mechanism, it consists of a large number of MIM junctions connected randomly in series and parallel over the film surface.

To couple energy into the diode efficiently a tungsten whisker with an etched tip is made to come in contact with a group of islands electrically. The sharp tip enhances the incident field and selects the desirable group of islands for diode action.

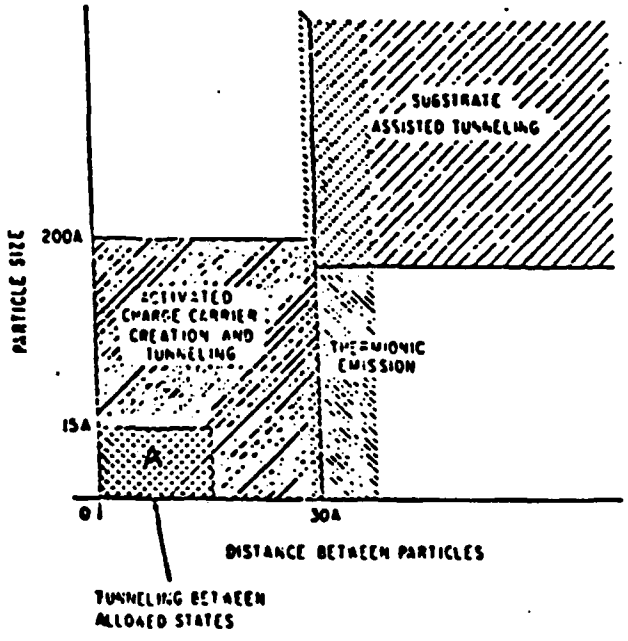

Figure 1. Region of island size and separation at which the proposed conduction mechanisms are most applicable.

CHAPTER II

ANALYSIS OF MIM FILM DIODE OPERATION

It is thought that useful properties of MIM diode arise from a non-linear current-voltage characteristic of the discontinuous metal film, together with the ability of the metal catwhisker to function as a receiving antenna converting the incident radiation to a voltage across the diode.

In this chapter we present calculation of the field generated at the tip of the catswhisker. We also discuss the electric conduction in discontinuous metal film based on tunneling of electrons through potential barriers between metal islands.

2.1 Theory of the Catswhisker Antenna Property

When the sharp tungsten whisker tip makes contact with the nickel oxide layer in MOM point-contact diode, very small amounts of stability will be achieved. The sharp tip is at the point of barely making contact with the oxide film, so that any vibration-induced variation in the separation between the tip and the post will lead to periodic breaking of contact and thus open circuit of the diode. This is diode resistance variation at the vibration frequency.

A tip with a slight bend or hook without blunting after contact with the oxide layer was a stabilization scheme introduced [14]. The controversy regarding hooking of the whisker tip without damage as a reliable method for stabilizing the MOM point-contact diode without significant

degradation of diode performance has been resolved [14]. The same concept is used in the MIM thin film diode, with the whisker playing the role of directional antenna. Experiments have shown that the tip of the etched whisker is responsible for field generation and current induction in the tungsten wire. The geometry of the tungsten wire in contact with the metal islands is shown in Figure 2.1. The tip of the etched whisker for different hook formation is shown in Figure 2.2.

Schelkunoff [10,11] has developed a general theory in which the antenna is viewed as a waveguide. This method facilitates the analysis of antennas with different geometries. Instead of describing the radiation field in terms of the natural oscillations of the antenna, the fields are expressed in transmission modes, which represent waves "guided" along the antenna. In Schelkunoff's analysis, the conical antenna is treated as a uniform transmission line, i.e., a system with a uniform characteristic impedence. Specifically the conical antenna acts as a waveguide for spherical waves propagating toward (receiving) or away (transmitting) from the cone apex. In our application of the conical antenna theory to the propagating of the fields on the whisker tip, we shall make use of Schelkunoff analysis and subsequent simplification introduced by Wolf and Kraus [12,13]. Thus in our conical antenna model, incoming spherical waves induce a current in the tip resulting in a voltage between the conical tip and metal film base.

As in the case of the field and the current distribution in a right circular cylinder, we shall need only those solutions of the wave equations for the electric and magnetic fields, $\bar{E}$ and $\bar{H}$ corresponding to the principal wave (TEM); all other wave solutions, of the compli-

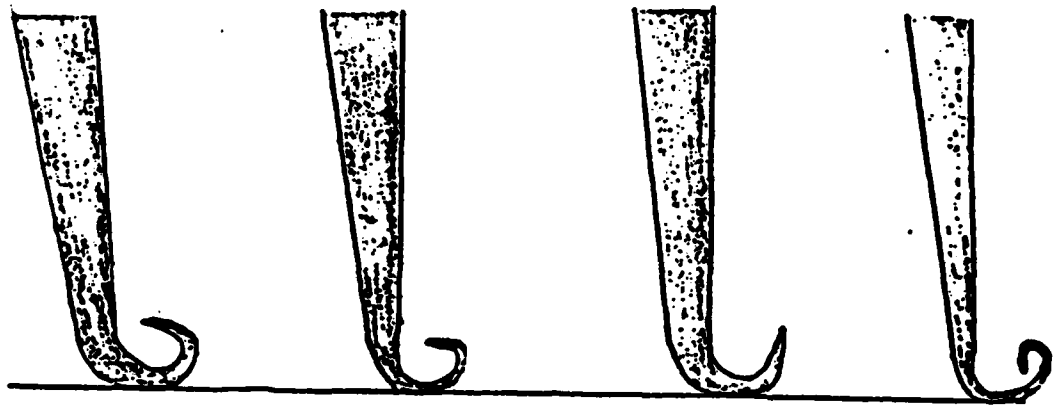

Figure 2.1. Shape of etched tips for different immersion depths after contact is made.

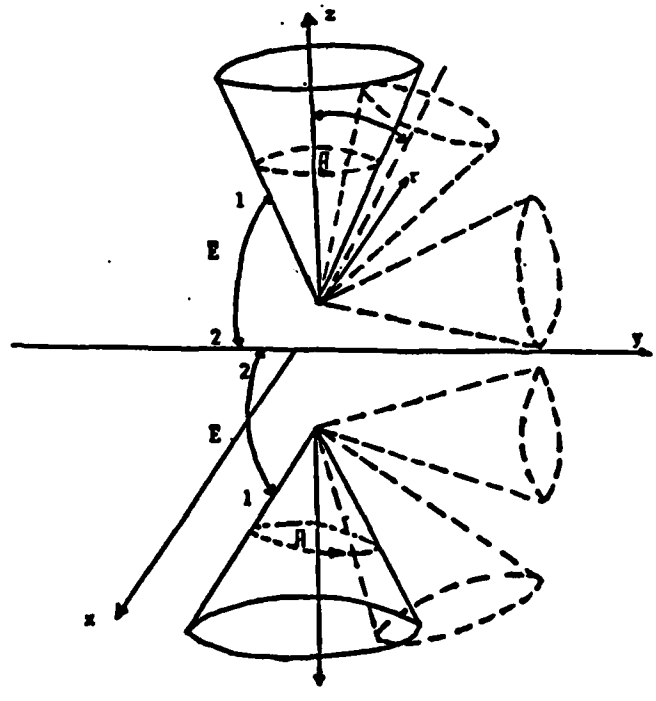

Figure 2.2 The tip of the etched whisker for different hook formation.

mentary waves, do not contribute to the detected voltage [15]. For the principal wave, both $\bar{E}$ and $\bar{H}$ are transverse, thus no radial component. The electric field lines form great circles passing through the polar axis (see Fig. 2.2). Since $\bar{E}$ has only a θ component, and $\bar{H}$ a ϕ component, the first Maxwell equation for harmonically time varing field

$$\nabla \times \mathbf{E} = -j\omega\mu\mathbf{H} \tag{1}$$

is in spherical coordinates

$$\frac{1}{r}\frac{\partial(rE_\theta)}{\partial r} = -j\omega\mu H_\phi \,, \tag{2}$$

where μ is the magnetic permeability of the medium

Similarly, the second Maxwell equation,

$$\nabla \times \mathbf{H} = j\omega\epsilon\mathbf{E} \tag{3}$$

where ϵ is the dielectric constant, reduces to

$$\frac{\partial(rH_\phi)}{\partial r} = -j\omega\mu(rE_\theta) \tag{4}$$

and

$$\frac{\partial(\sin\theta\, H_\phi)}{\partial\theta} = 0 \,. \tag{5}$$

A wave equation for $(r\bar{H}\phi)$ is derived by differentiating Eq. (4) with respect to r and using Eq. (3):

$$\frac{\partial^2(rH_\phi)}{\partial r^2} = -\omega^2\mu\epsilon(rH_\phi) \,. \tag{6}$$

It is seen from Eq. (5) that H_ϕ has the form

$$H_\phi \propto \frac{1}{\sin\theta} \,. \tag{7}$$

A solution which satisfies both Eqs. (6) and (7) is

$$H_\phi = \frac{1}{r \sin\theta} H_0 e^{\mp i\beta r} \tag{8}$$

where $\beta = \omega\sqrt{\mu\varepsilon} = 2\pi/\lambda$, and the upper sign refers to a spherical wave approaching the tip and the lower sign denotes an outgoing spherical wave.

The electric and magnetic fields of a TEM wave are related by the intrinsic impedence Z_0 of the medium. Thus we have

$$E_\theta = Z_0 H_\phi = \frac{Z_0}{r \sin\theta} H_0 e^{\mp i\beta r} \tag{9}$$

where Z_0 is 120 ohms for free space.

When the tip apex is close to the base, it is simple to obtain the voltage between say point 1 on the tip and point 2 on the base (see Fig. 2.2). The voltage generated between these two points is given by the line integral for $\bar{E}$,

$$V(r) = \int_{\theta_{hc}+\theta_r}^{\frac{\pi}{2}} E_\theta \, r \, d\theta \tag{10}$$

Where Θ_{hc} is the half cone angle and Θ_r is the angle between the half cone and the Z-axis. Equation (10) is integrated, using Eqs. (8), and (9)

$$V(r) = Z_0 H_0 e^{\mp i\beta r} \int_{\theta_{hc}+\theta_r}^{\frac{\pi}{2}} \frac{d\theta}{\sin\theta}$$

$$V(r) = 2 Z_0 H_0 e^{\mp i\beta r} \ln \cot \frac{\theta_{hc}+\theta_r}{2} \tag{11}$$

The net current I(r) on the cone at a distance r from the tip may be obtained from Ampere's law;

$$I(r) = \int_0^{2\pi} H_\phi r \sin\theta \, d\phi = 2\pi r H_\phi \sin\theta \tag{12}$$

$$I(r) = 2\pi H_0 e^{\mp i\beta r}$$

The radiation pattern of the catswhisker in MIM diode varies over a wide range of wavelengths (5cm.- 10.6μm). In the low frequency range, the whisker tip acts as a short antenna and the radiation pattern is not highly directional. On the other hand, at higher frequencies (infrared and laser frequency) the whisker tip becomes long wire antenna and the radiation pattern is highly directional.

2.2 Tunnel-Effect in the MIM (Metal-Insulator-Metal) Structure

Normally, the only way an electron can pass from one electrode to the other is if it has sufficient energy to overcome the barrier existing at the metal insulator interface, that is, if it can enter the conduction band of the insulator, by thermionic emission. If the energy of the electron is less than the interfacial barrier height, classical physics predicts that the electron cannot penetrate the barrier. In quantum theory, however the quantum mechanical wave function, $\psi(x)$, of the electron has finite values within the barrier (see Fig. 2.3), and, since $\psi(x) * \psi(x)dx$ is the probility of finding the electron within the incremental range X to X + dX, this means that the electron can penetrate the forbidden region of the barrier. The wave function decays rapidly with depth of penetation of the barrier from the electrode-insulator interface, and is essentially zero at the opposite interface, for the barrier of macroscopic thickness, indicating zero probability of finding the electron there (see Fig. 2.3a). However, if the barrier is very thin (<50 Å), the wave function has a nonzero value at the opposite interface, so that there is finite probability that the electron can pass from one electrode to the other by penetrating the barrier (see Fig. 2.3b), via

Figure 2.3. Schematic representation of the tunnel effect. (a) for a thick barrier. (b) for a very thin barrier.

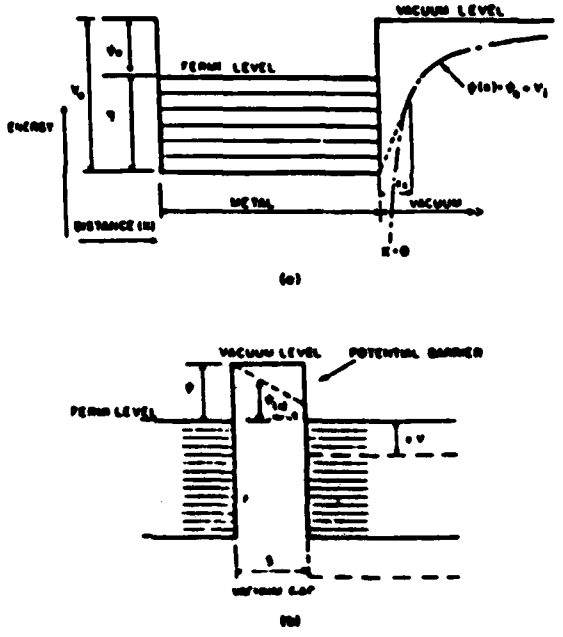

Figure 2.4 Potential energy diagram of (a) metal-vacuum interface after Sommerfeld, and (b) metal-vacuum-metal interface.

the tunneling process.

In the Sommerfeld [16] free-electron theory for metals, it is assumed that the free electrons (the electrons responsible for electrical characteristics of metals) move in a constant potential environment within the metal. Figure 2.4 is the energy band diagram of the Sommerfeld model; the metal is represented by a potential energy well of depth V_o; the vacuum level represents the energy of an electron at rest outside the metal. In Fig. 2.4a the potential barrier is shown as an abrupt step; later a more realistic model will be adopted. At 0°K, the electrons which exist in discrete energy levels, fill up the well to the Fermi level η. The distance $\psi = V_o - \eta$ from the Fermi level to the vacuum level is known as the work function of the metal, and represents the minimum energy required to free electrons from the interior of the metal at 0°K.

Under equilibrium conditions, two similar electrodes separated by a distance S is shown in Fig. 2.4b. There exists a potential barrier of width S and constant height ψ above the Fermi level. When a potential difference V exists between the electrodes, the Fermi levels are separated by an energy eV as shown in Fig. 2.4b (dotted line). The barrier height is a linear function of the distance within the barrier;

$$\psi(X) = \psi - eVX/S$$

$D(E_x)$ is the probability that an electron can penetrate a potential barrier of height V(X) in the X direction as shown in Fig. 2.5 and is given by the well known WKB approximation [17].

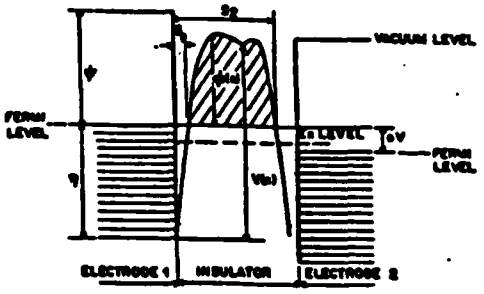

Figure 2.5. General potential barrier in insulating film between two metal electrodes.

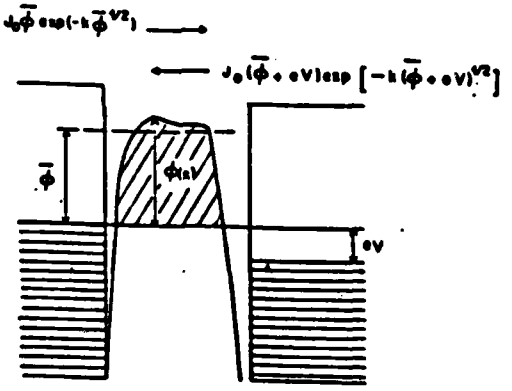

Figure 2.6. Illustration of Eq. (32) showing current flow between the electrodes.

$$D(E_x) = \exp\left\{-\frac{4\pi}{h}\int_{s_1}^{s_2}[2m(V(x)-E_x)]^{1/2}dx\right\}. \tag{13}$$

Where $E_x = mV_x^2/2$ - energy component of the incident electron in the X direction.

m = mass of electron

v = voltage across film

h = Planck's constant

s = thickness of insulating field

$s_2 - s_1$ = width of potential barrier at Fermi level

N_1 electrons tunneling through the barrier from electrode 1 to electrode 2 as given by

$$N_1 = \int_0^{v_m} v_x n(v_x) D(E_x) dv_x = \frac{1}{m}\int_0^{E_m} n(v_x) D(E_x) dE_x, \tag{14}$$

Where E_m is the maximum energy of the electrons in the electrode, and $n(v_x)dv_x$ is the number of electrons per unit volume with velocity between v_x and $v_x + dv_x$. For an isotropic velocity distribution which is assumed to exist inside the electrodes, the number of electrons per unit volume is given by

$$n(v)dv_x dv_y dv_z = (2m^3/h^3) f(E) dv_x dv_y dv_z, \tag{15}$$

where f(E) is the Fermi-Dirac distribution function. Consequently, from Eq. (15)

$$n(v_x) = \frac{2m^3}{h^3} \int \int_{-\infty}^{\infty} f(E)\,dv_y\,dv_z$$
$$= \frac{4\pi m^3}{h^3} \int_0^{\infty} f(E)\,dE_v. \qquad (16)$$

Where

$$v_r^2 = v_y^2 + v_z^2,$$
$$E_r = mv_r^2/2.$$

Substitution of Eq. (16) in Eq. (14) yields

$$N_1 = \frac{4\pi m^2}{h^3} \int_0^{E_m} D(E_x)\,dE_x \int_0^{\infty} f(E)\,dE_r. \qquad (17)$$

The number of electrons N_2 tunneling from electrode 2 to electrode 1 is determined in a similar manner. The tunneling probility $D(E_x)$ is the same in either direction, and if electrode 2 is at positive potential V with respect to electrode 1, the Fermi-Dirac function is written as $f(E + eV)$; therefore,

$$N_2 = \frac{4\pi m^2}{h^3} \int_0^{E_m} D(E_x)\,dE_x \int_0^{\infty} f(E+eV)\,dE_r. \qquad (18)$$

The net flow of electrons N ($=N_1 - N_2$) through the barrier is

$$N = \int_0^{E_m} D(E_x)\,dE_x$$
$$\times \left\{ \frac{4\pi m^2}{h^3} \int_0^{\infty} [f(E) - f(E+eV)]\,dE_r \right\}. \qquad (19)$$

Writing

$$\xi_1 = \frac{4\pi m^2 e}{h^3} \int_0^\infty f(E)\,dE_x,$$

and

$$\xi_2 = \frac{4\pi m^2 e}{h^3} \int_0^\infty f(E + eV')\,dE_x,$$

and $\xi = \xi_1 - \xi_2$, Eq.19 becomes

$$J = \int_0^{E_m} D(E_x)\xi\,dE_x. \tag{20}$$

Writing $V(x) = \eta + \psi(x)$ with reference to Figure 2.5, Eq. (13) becomes

$$D(E_x) = \exp\left[-\frac{4\pi}{h}(2m)^{\frac{1}{2}} \int_{x_1}^{x_2} (\eta + \varphi(x) - E_x)^{\frac{1}{2}} dx\right]. \tag{21}$$

Integrating Eq. (21) using Eq. (B5) from Appendix B we arrive at

$$D(E_x) \simeq \exp[-A(\eta + \bar{\varphi} - E_x)^{\frac{1}{2}}], \tag{22}$$

where $\bar{\psi}$ is the mean barrier height above the Fermi level of the negatively biased electrode

$$\bar{\varphi} = \frac{1}{\Delta s} \int_{x_1}^{x_2} \varphi(x)\,dx,$$

$$A = (4\pi\beta\Delta s/h)(2m)^{\frac{1}{2}};$$

and β is defined in Appendix B. At 0°K, ξ_1 and ξ_2 are given by

$$\xi_1 = (4\pi me/h^3)(\eta - E_x)$$

and

$$\xi_2 = (4\pi me/h^3)(\eta - E_x - eV').$$

so that

$$\zeta=\begin{cases}(4\pi mc/h^3)(eV) & 0<E_x<\eta-eV\\ (4\pi mc/h^3)(\eta-E_x) & \eta-eV<E_x<\eta\\ 0 & E_x>\eta\end{cases}. \tag{23}$$

Substitution of Eqs. (22) and (23) in Eq. (20) gives

$$J=\frac{4\pi mc}{h^3}\left\{eV\int_0^{\eta-eV}\exp[-A(\eta+\bar{\varphi}-E_x)^{1/2}]dE_x + \int_{\eta-eV}^{\eta}(\eta-E_x)\exp[-A(\eta+\bar{\varphi}-E_x)^{1/2}]dE_x\right\}. \tag{24}$$

To facilitate integration, Eq. (24) is written in the form

$$J=\frac{4\pi mc}{h^3}\left\{eV\int_0^{\eta-eV}\exp[-A(\eta+\bar{\varphi}-E_x)^{1/2}]dE_x - \bar{\varphi}\int_{\eta-eV}^{\eta}\exp[-A(\eta+\bar{\varphi}-E_x)^{1/2}]dE_x + \int_{\eta-eV}^{\eta}(\eta+\bar{\varphi}-E_x)\times\exp[-A(\eta+\bar{\varphi}-E_x)^{1/2}]dE_x\right\}. \tag{25}$$

The first of the integrals in Eq. (25) yields

$$(8\pi mV/h^3)(e/A)^2\{[A(\bar{\varphi}+eV)^{1/2}+1]\exp[-A(\bar{\varphi}+eV)^{1/2}] - [A(\bar{\varphi}+\eta)^{1/2}+1]\exp[-A(\bar{\varphi}+\eta)^{1/2}]\}. \tag{26}$$

The second term in the braces is negligible compared to the first term as usually, $A(\bar{\psi} - eV)^{\frac{1}{2}} >> 1$. Thus Eq. (26) reduces to

$$(8\pi me^2/h^3A)1'(\bar{\varphi}+eV')^1 \exp[-A(\bar{\varphi}+eV')^1]. \tag{27}$$

The second integral in Eq. (25) is of the same form as the first, and is similarly approximated to

$$-(8\pi me/h^3A^3)\bar{\varphi}\{[A\bar{\varphi}^1+1]\exp(-A\bar{\varphi}^1) - [A(\bar{\varphi}+eV)^1+1]\exp[-A(\bar{\varphi}+eV)^1]\}. \tag{28}$$

The third integral of Eq. (25) has the form

$$\int z^3 e^{-Az}dz = -e^{-Az}\left(\frac{z^3}{A}+\frac{3z^2}{A^2}+\frac{6z}{A^3}+\frac{6}{A^4}\right), \tag{29}$$

where $z^2 = \eta + \bar{\varphi} - E_x$.

The third and fourth terms in the parentheses in Eq. (29) are negligible in comparison to the first two; so that the third integral in Eq. (25) becomes

$$\begin{aligned}(8\pi me/h^3A)\{&\bar{\varphi}^1\exp(-A\bar{\varphi}^1) \\ &-(\bar{\varphi}+eV)^1\exp[-A(\bar{\varphi}+eV)^1]\} \\ &+(8\pi me/h^3A)(3/A)\{\bar{\varphi}\exp(-A\bar{\varphi}^1) \\ &\quad -(\bar{\varphi}+eV)\exp[-A(\bar{\varphi}+eV')^1]\}.\end{aligned} \tag{30}$$

Summation of Eqs. (27), (28) and (30) yields

$$J=(e/2\pi h)(\beta\Delta s)^{-2}\{\bar{\varphi}\exp(-A\bar{\varphi}^{\frac{1}{2}}) - (\bar{\varphi}+eV)\exp[-A(\bar{\varphi}+eV)^{\frac{1}{2}}]\}. \tag{31}$$

Equation (31) can be expressed in the following forms:

$$J=J_0\{\bar{\varphi}\exp(-A\bar{\varphi}^{\frac{1}{2}}) - (\bar{\varphi}+eV)\exp[-A(\bar{\varphi}+eV)^{\frac{1}{2}}]\}, \tag{32}$$

where

$$J_0=e/2\pi h(\beta\Delta s)^2.$$

Equation (32) has the advantage that it can be applied to any shape of potential barrier provided the mean barrier height is known, or alternatively, if the current-voltage characteristic of a tunnel junction is known, the mean barrier height can be determined.

Equation (32) can be interpreted as a current density $J_0\exp(-A\bar{\psi}^{\frac{1}{2}})$ flowing from electrode 1 to electrode 2 and a current density $J_0(\bar{\psi} + eV)$ $\exp[-A\bar{\psi} + eV)^{\frac{1}{2}}]$ flowing from electrode 2 to electrode 1 resulting in a net current density J given by Eq. (20) (see Figure 2.6).

CHAPTER III

DISCONTINUOUS MIM FILM DIODE STRUCTURE

3.1 MOM Diode Background Technology

Metal-Oxide-Metal (MOM) diodes are the fastest detector known. They are used in the frequency range from microwave to submillimeter wave and infrared spectral regions. Submillimeter waves as well as infrared frequency mixing and recitification with point-contact MOM diodes have been achieved [18, 19, 20, 21], and detection in the optical range using MOM diodes has been reported [22,23].

The responsivity and detectivity of MOM diodes are lower than those of cooled quantum detectors [24]. However ultra fast rise time of MOM diodes makes them attractive devices for a variety of applications. Absolute frequency measurements have performed up to 150THz using MOM junctions as harmonic mixers. They are also needed for the observation of fast laser pulses and in broad-band hetrodyne systems used in laser radar and optical communication.

MOM diodes are mostly used in the form of conventional point-contact diodes. A thin whisker is etched electrolytically and serves as a long wire antenna. The resulting sharp tip is pressed against a polished metalic base (see Fig. 3.1). The natural oxide layer on the base material forms the potential barrier for the tunneling electrons. Although these diodes are relatively easy to build, serious drawbacks hinder a more widespread usage. The responsivity of early point-contact

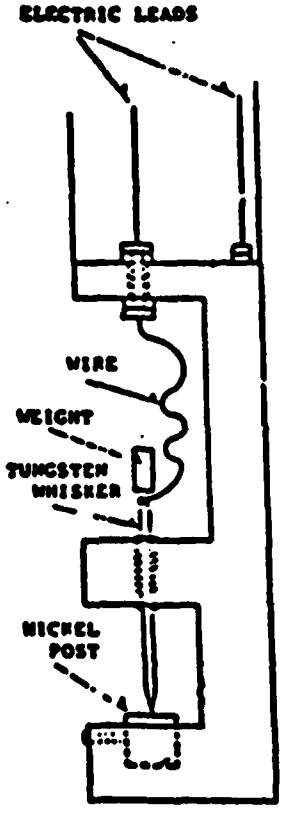

Figure 3.1. Conventional point-contact diode structure

diodes is unstable, and even exhibits polarity reversal during operation. Early MOM detectors are also known to suffer both from microphony and electrical transients. Since the relevent parameters, such as oxide thickness and junction area cannot be controlled, the characteristics are not reproducible from one diode to another. Furthermore, stable and reproducible antenna configurations are difficult to realize with thin, free standing whisker.

Marked improvement was reported on the stability of MOM point-contact diode by deliberate hooking of the whisker tip [14, 25,26](see Fig. 3.2) The bent or hooked tip has often been encountered by workers in this field, but viewed negatively because of its uncontrollability and the possibility of increased contact area, thus increased capacitance and reduced local field enhancement. However, it has also been argued that the simultaneous reduction in diode resistance due to increased contact area may approximately compensate the increase in capacitance, so that predicted RC degradation is debatable. It turned out that diverting the sharp tip from the contact area also had negligible effect on local field enhancement.

From a physical point of view, hooking provides some cushioning for mechanical vibrations, a free end for thermal expansion and contraction and a rounded bend in the oxide junction area with reduced susceptibility to electrical charge buildup.

Planar metal-insulator-metal (MIM) structures [4] have been proposed as alternative structures to the metal-oxide-metal (MOM) point-contact diode. The printed circuit version [27] still retains the sharp tip

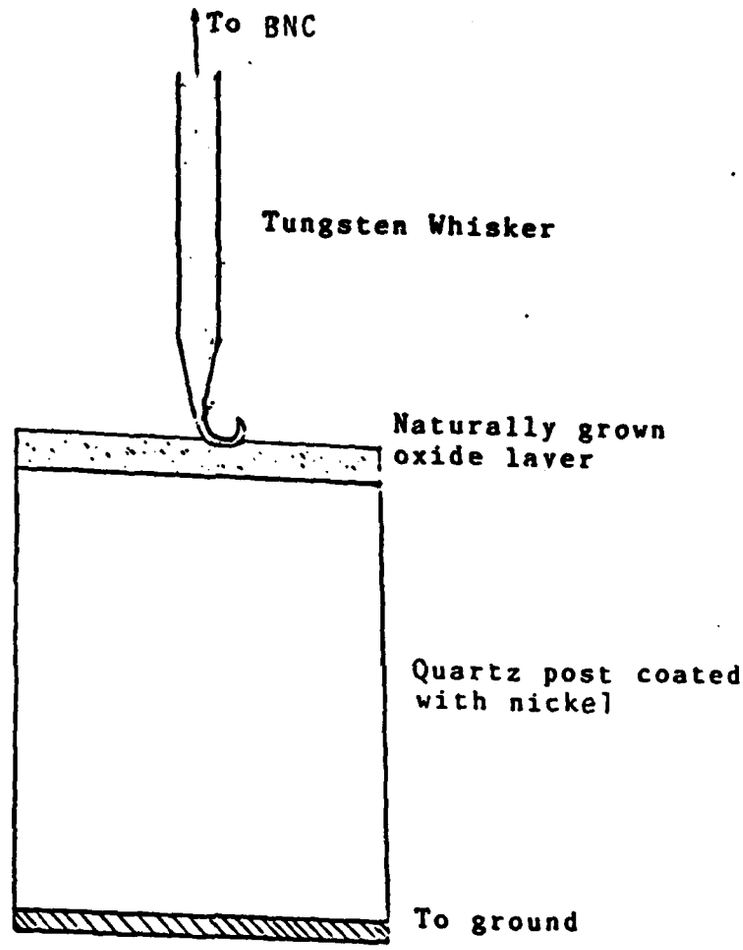

Figure 3.2. MOM Point-contact diode structure.

structure and thus inherently sensitive to thermal and electrical instabilities. These instabilities were absent in the discontinuous MIM film diode fabricated by vacuum sputtering of various types of metals on to glass plate. Due to the highly nonuniform nature of discontinuous metal films, the film diode was composed of chips electrically interconnected into arrays. This was an attempt to select desirable patches of islands and interconnect them in such a manner as to achieve a multi-chip diode with the proper resistance. Thus, low resistivity chips were connected in series to fully utilize the desirable feature of proximity of islands. High resistivity chips were connected in parallel to arrive at an optimum overall resistance (see Fig. 3.3).

The success of planar diodes using discontinuous MIM films and island array was limited to only assurance of stability. Responsivity of the diode suffers from the absence of the long wire antenna of the point-contact version. Chip array interconnection is highly unpredictable so that diode characteristics are not reproducible and repeatable.

3.2 Alternative Structure of MIM Film Diode

After extensive research, we have come to the conclusion that the long whisker antenna can be reinstated if proper design considerations are taken. It is thus our aim to fabricate and test a hybrid planar diode package that consists of discontinuous nickel film deposited on a glass substrate with a tungsten whisker antenna. In this case, the metal islands are separated by naturally grown oxide layers of dimensions that allow for tunneling; the tungsten whisker with an etched tip is caused to make electrical contact with a select group of islands to

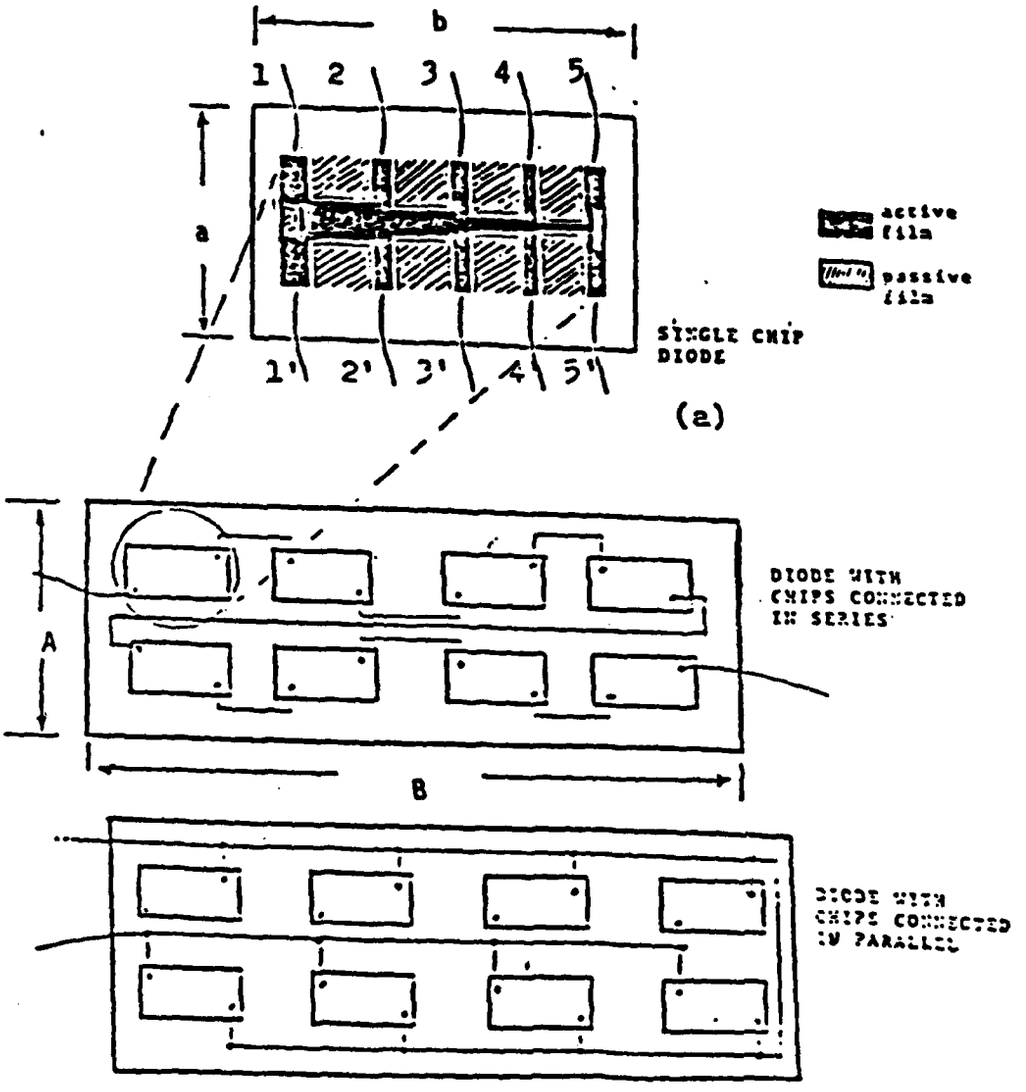

Figure 3.3 (a) Single chip with leads: (b) Chip arrays in series and parallel.

A,B dimensions conform to waveguide dimensions; a,b dimensions typically in the range of a few millimeters.

enhance the incident field on the islands and select the desirable group of islands for diode action.

Patches of deposited nickel islands are carefully preselected, then they are isolated and removed with the glass substrate, which is in turn glued to another glass plate. The etched tungsten whisker is laid flat on the latter glass plate and silver cemented to it. The stem portion of the whisker is bent such that the etched tip makes firm contact with the nickel film patch. The contact pressure must be such that the tip penetrates the oxide layer of the film and make electrical contact with the metal islands. The tip will be hooked in the penetration process (see Fig. 3.4). Then the whisker-enhanced film diode is packaged in a waveguide.

3.3 Film Characteristics

In our attempt to construct discontinuous metal film diode as high frequency detector with low noise, high sensitivity and stability, it stands to reason to fabricate films in which direct tunneiling is the dominant conduction mechanism. It is known [26] that films of palladium or platinum-palladium deposited on glass substrates provide stable islands of extremely small size. However, these films normally present high sheet resistance of several megohms and low sensitivity. Such high diode resistance is easily loaded by external detection circuits.

A multi-layer film structure was therefore suggested, consisting of palladium-platinum film deposited on gold discontinuous film. Test results indicated Pd-Au films were superior in performance to Pd film [27] due possibly to the difference in the work function of dissimilar

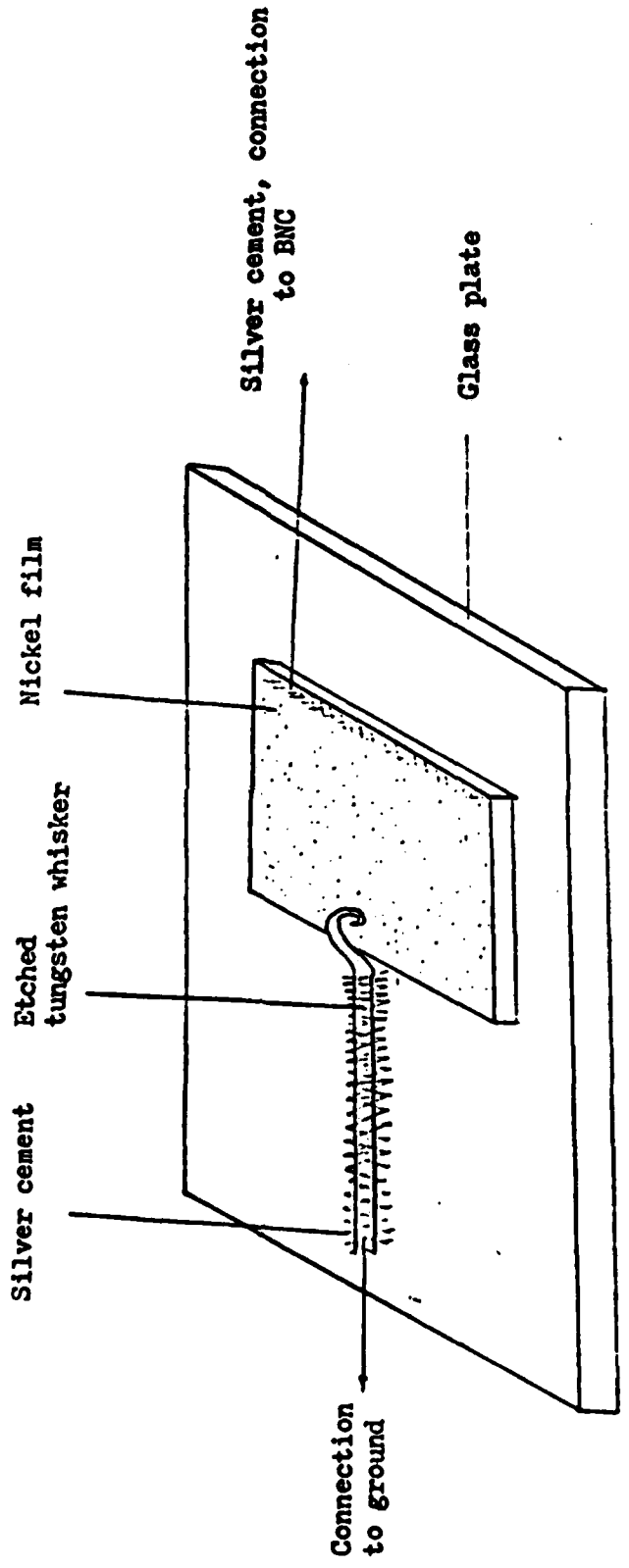

Figure 3.4. Sketch of film diode and mount.

metals. However, film resistance was too low for extraction of detectable signal from the film. Finally nickel was selected [21] as the film element in the planar MIM discontinuous film diode, since its natural oxide layer was very thin and of extremely high sheet resistance, as learned from our work on MOM point contact diode [24]. Thus, high density nickel islands can be deposited that will be separated by very thin oxide layers.

3.4 Film Deposition

Glass slides cleaned with Fisher biodegradable sparkleen solution was used as the film substrate. Such slides were boiled in the solution and transferred into an ultrasonic cleaner and cleaned for 30 minutes. The slide was then rinsed in boiling deionized water, and then ultrasonically cleaned for another 30 minutes. The slide was removed and blown dry with nitrogen gas. The dried slide was then mounted in the model SEM-8620 sputtering unit manufactured by Materials Research Corporation. The sample was placed on the J head, while the target was made the cathode. The sputtering unit was then vacuum sealed and pumped down to a vacuum pressure of 10^{-6} Torr. The system was then backfilled with an inert gas (argon) to 5 microns as the sputtering plasma. The metal target was pre-sputtered as degased to remove impurities. The sputtering power then set and sputtering was performed over a prescribed period of time. The slide with the deposited film was then removed for film resistance check.

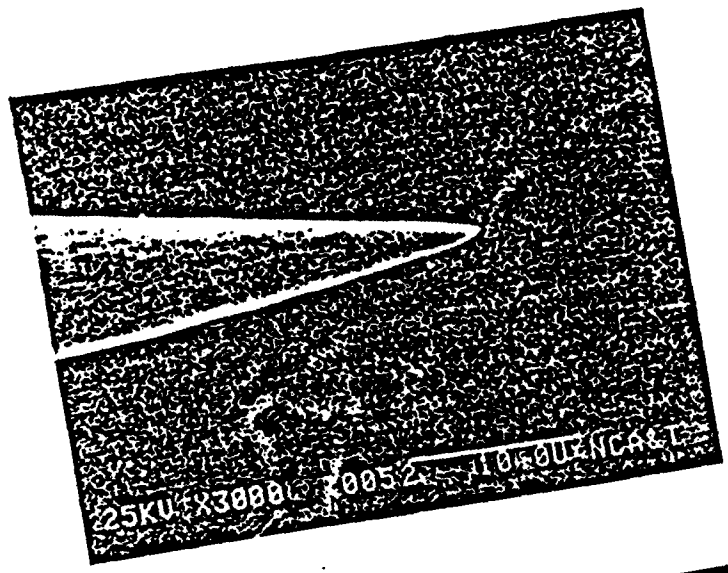

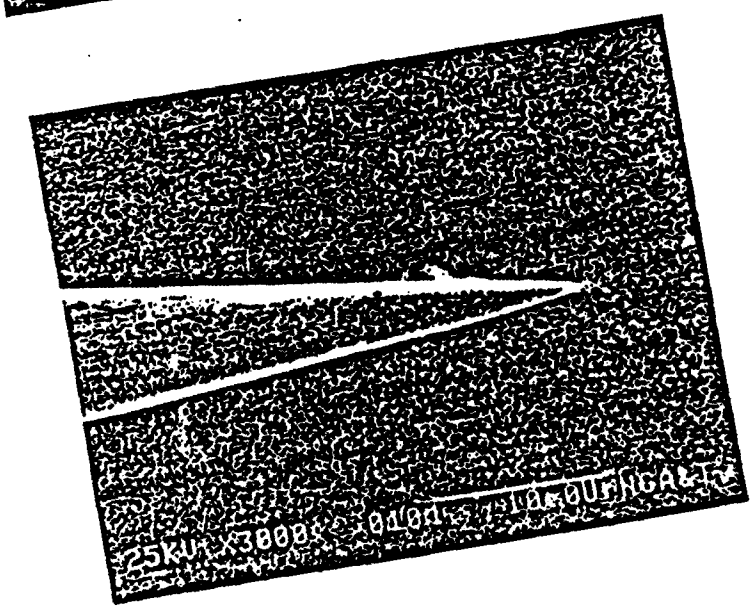

Figure 3.5. SEM Pictures of etched tungsten tips (X3000 magnification).

3.5 Electrolytic Etching of the Catswhisker

The 3N KOH solution was prepared with distilled water. The twenty five μm diameter tungsten wire to be etched served as one electrode, while a copper plate, covering the bottom of the bath that contained the KOH solution, served as the other electrode. An 8v Ac was applied directly to the electrodes, with precautions taken to reduce etching circuit resistance to a minimum of 1-2Ohms. Circuit resistance variation due to the introduction of metering or poor contact between the tungsten wire to be etched and the vice that held the wire in a firm grip was often reflected in significant variation in the etching time. The shape of the etched tip was then controlled by the depth of immersion of the wire in the electrolytic solution. Two typical etched-tips for two different immersion depths are shown in Fig. 3.5.

3.6 Catswhisker Tip Contacting or Hooking Process

The contact process was characterized by two parameters; contact pressure and amount of tip hooking without undesirable blunting or damage. The distance between the vertical elevation of the film plate and the plate that the tungsten wire is mounted, can be varied so as to vary the contact pressure of the whisker tip. The limit was reached when the whisker shaft began to buckel and hooking was initiated. The ultimate contact pressure was the important parameter, which was in turn controlled by the amount of hooking.

3.7 Diode Packaging

MIM discontinuous film diodes were tested at X band due to availability

of tunable sources with adequate power. X-band waveguide was used for the diode mount. The open W/G mount can be used for incident radiation at higher frequencies.

Two short sections of the waveguide were cut from X-band waveguides. The first section (A) was to serve as the BNC connector mount, while the other section (B) was to serve as the diode housing. Section A was the lid for section B. One face of the waveguide section A was removed to create an open structure for the installation of BNC panel receptacle on the remaining face. This served as the signal output port of the diode. The waveguide section B was sliced into halves. This exposed the inside of the waveguide for ease of diode mounting. A plane glass plate of the inside dimension of the waveguide was glued to the base of the lower half of section B. This would serve as the securing wall for the glass substrate with the chips and wire leads. The glass substrate was glued to this wall. During the test, the upper half and lower half of section B were rejoined and temporarily clamped together to form a standard waveguide (see Figs. 3.6, 3.7 and 3.8). The other end of the etched tungsten wire was silver cemented to the base of the waveguide, which served as ground. A lead wire cemented to the BNC was shaped into a coil spring with the other end cemented to the film (see Fig. 3.6).

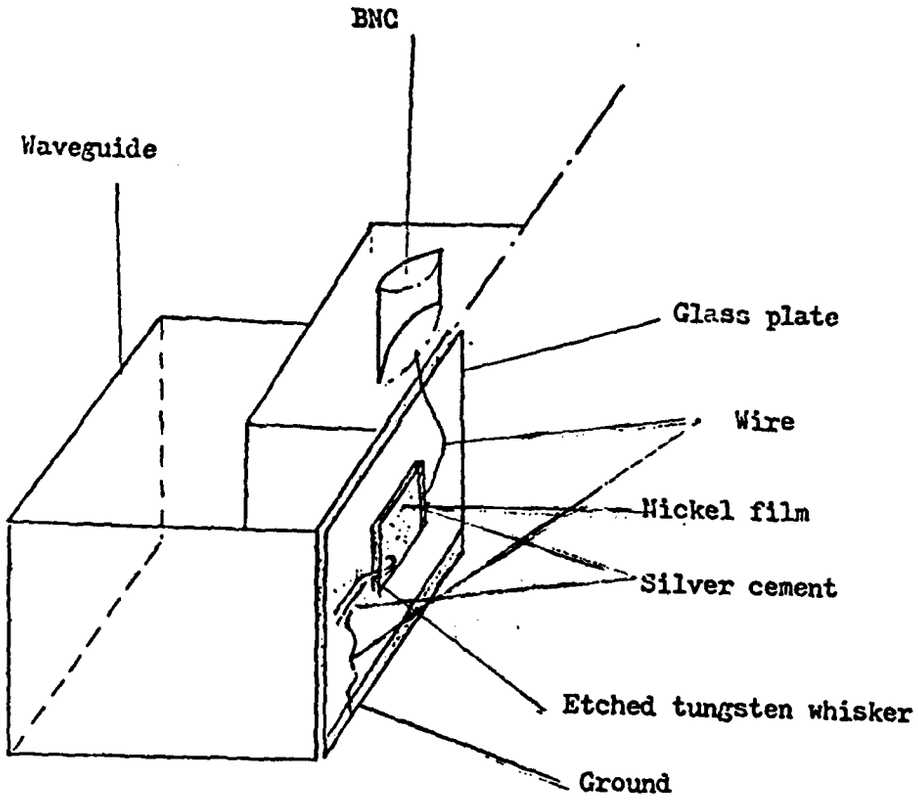

Figure 3.6. Cross sectional view of waveguide packaging.

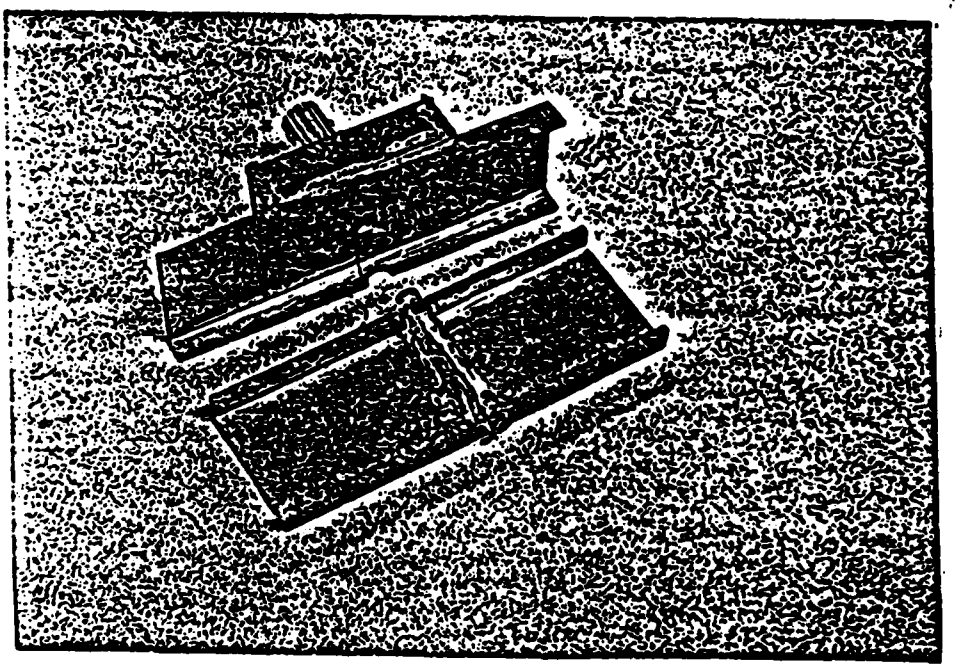

Figure 3.7. Mounting of the film diode inside the X-band waveguide.

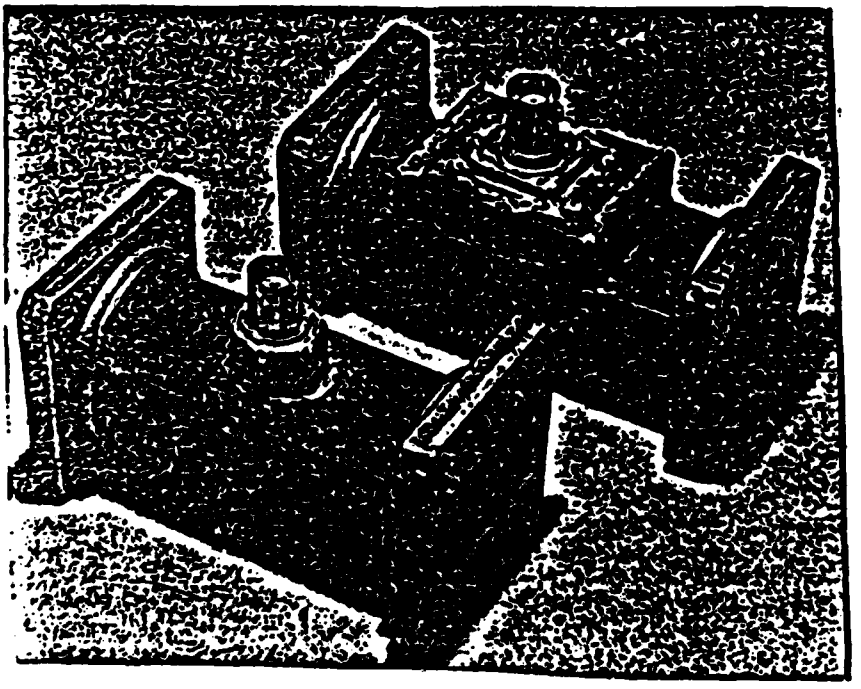

Figure 3.6 Waveguide diode packaging.

CHAPTER IV

TEST RESULTS ON MIM FILM DIODE

4.1 Film Selection

Film deposition is done in different conditions. The major variables in film deposition are the sputtering power and sputtering time. After deposition is completed, to eliminate film patches with very high sheet resistance (>10 KΩ) or very low resistance (<1 KΩ), the I-V characteristic of each patch is examined with gold tip probes. Since film deposition is nonuniform throughout the glass substrate, in the first stage of film selection we use the average resistance of the films.

The I-V curves of Ni films which deposited in different conditions are shown in Figure 4.1. The results are summarized in Table 4-1. According to the results, the optimum Ni film (4 KΩ<R< 10 KΩ) can be produced at 50W sputtering power and 30 sec sputtering time. Under these conditions, film resistance is in the range of 10KOhm. This is the range of high island density, hence narrow oxide layer between island, thus high tunneling probility.

The film patches are removed with their glass substrates intact. Again the I-V characteristic of each film patch is examined to make sure that the film resistance is in the desirable range (4 KΩ<R< 10KΩ). Now the film patches are ready to be mounted in the X-band waveguide.

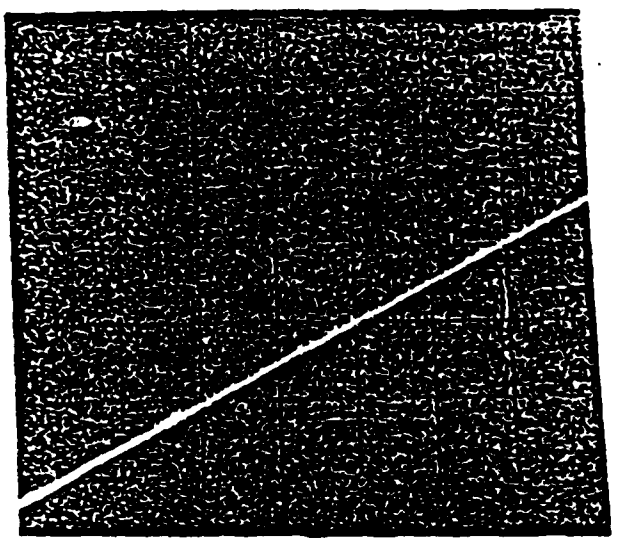

Figure 4.1a. I-V curve of (100W, 30 sec.) Ni film. (R = 1.6 KΩ)

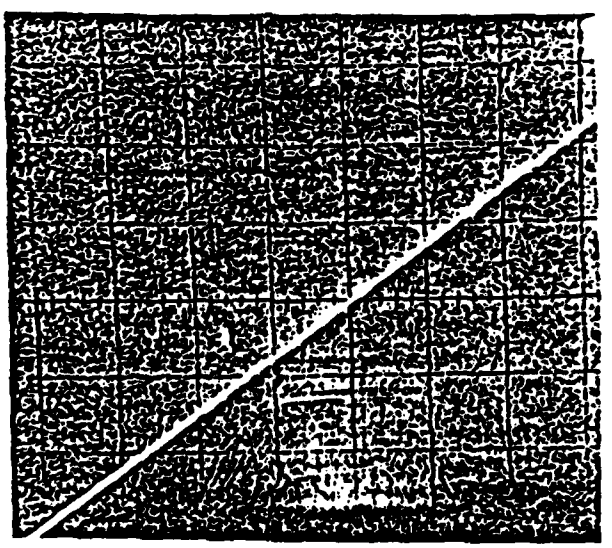

Figure 4.1b. I-V curve of (100W, 15 sec.) Ni film. (R = 120 KΩ)

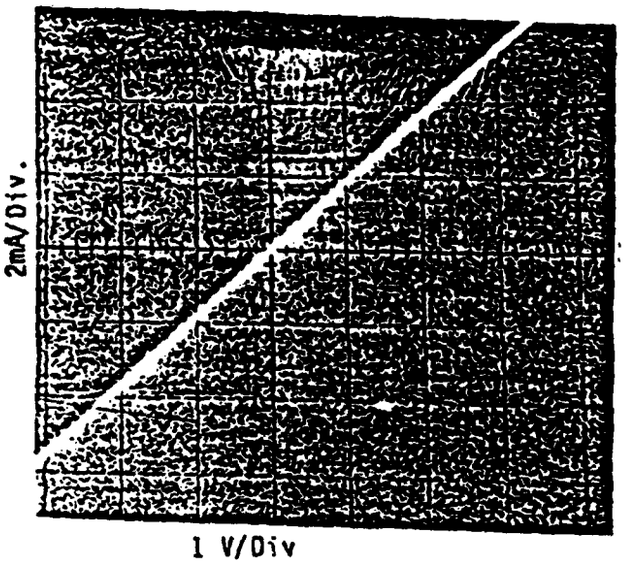

Figure 4.1c. I-V curve (50W, 45 sec.) of Ni film. (R = 500 Ω)

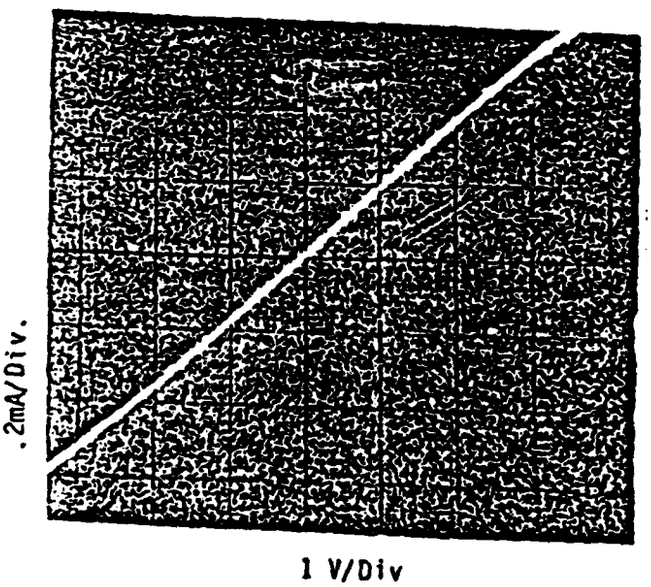

Figure 4.1d. I-V curve (50W, 30 sec.) of Ni film (R = 5 KΩ)

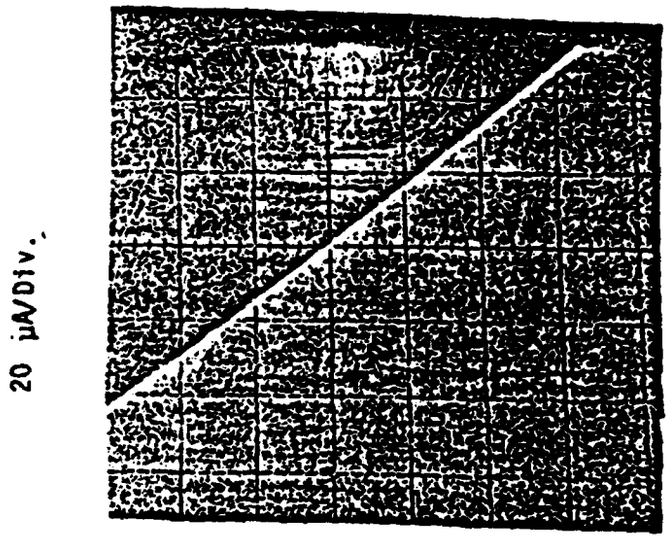

Figure 4.1e. I-V curve (50W, 20 sec.) of Ni film. (R = 50 K Ω)

TABLE 4-1. RESISTANCE OF Ni FILMS IN FIVE DIFFERENT DEPOSITION CONDITIONS

SPUTTERING POWER	DEPOSITION TIME	FILM TYPE	FILM RESISTANCE
100 W	30 sec	Ni (A)	2.1 KΩ - 700 Ω
100 W	15 sec	Ni (B)	110 KΩ - ∞
50 W	45 sec	Ni (C)	1.2 KΩ - 220Ω
50 W	30 sec	Ni (D)	4 KΩ - 10 KΩ
50 W	20 sec	Ni (E)	14 KΩ - ∞

4.2 Selection of Etched Tungsten Whisker

Since sufficient contact pressure must be exerted on the whisker tip before a hook would form, it is thus clear that tip with small slender ratio (the ratio of the shaft length to tip diameter), i.e., sharp tips with short shaft, will not hook readily and are thus more suceptible to blunting or damage. On the other hand, tips with large or moderate slender ratios can hook without blunting. Thus there is an optimum shape and contact pressure for the best hook performance. There is an upper limit to the slender ratio, above which the whisker is too slender and large radius hooks are formed with unpredictable contact pressure.

Figure 4.2a shows an etched tip of a small slender ratio. Upon contact with metal islands, no hooking was observed (see Fig. 4.2b). This is defined as a damaged or blunted tip. Such an MIM film diode exhibited totally unsatisfactory detection performance when tested at 10GHz, i.e., the diode has low responsivity and is unstable. Figure 4.3a and 4.4a show etched tips with a proper slender ratio that produce hooking without tip blunting or damage, as seen in Fig. 4.3b and 4.4b.

A systematic study was conducted by us [14] to arrive at a slender ratio for best response and stability of the MOM point-contact diode with an undamaged hook. Having arrived at the appropriate parameters, optimum tips were repeatedly fabricated for the MIM film diode.

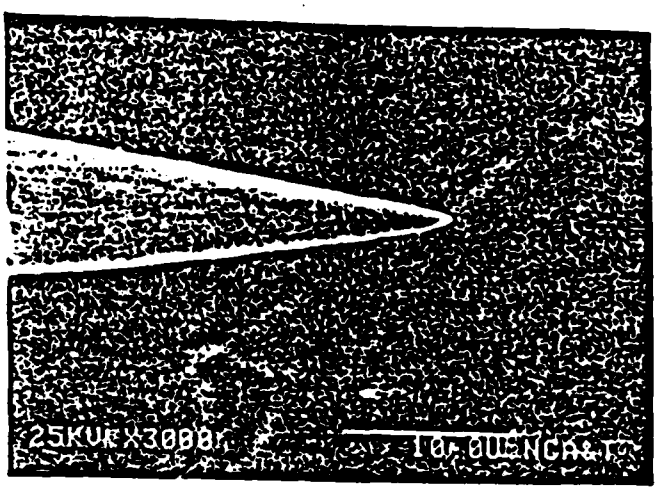

(a)

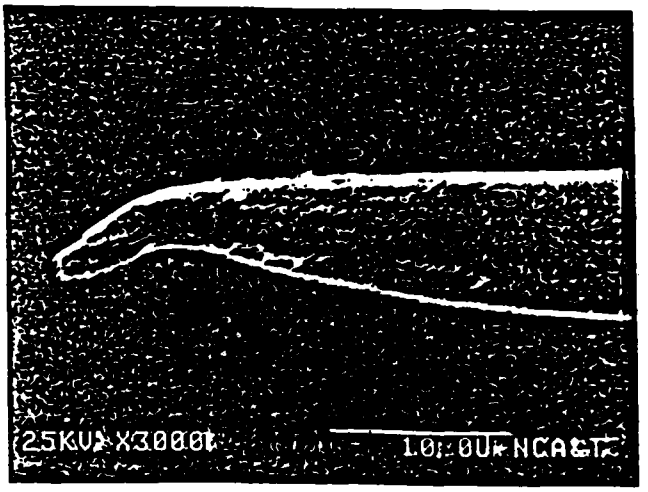

(b)

Figure 4.2. Photographs of etched tip before and after blunting (using SEM).

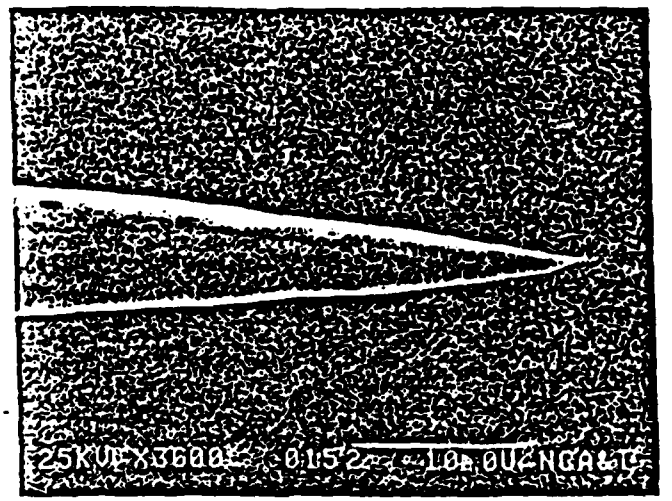

(a)

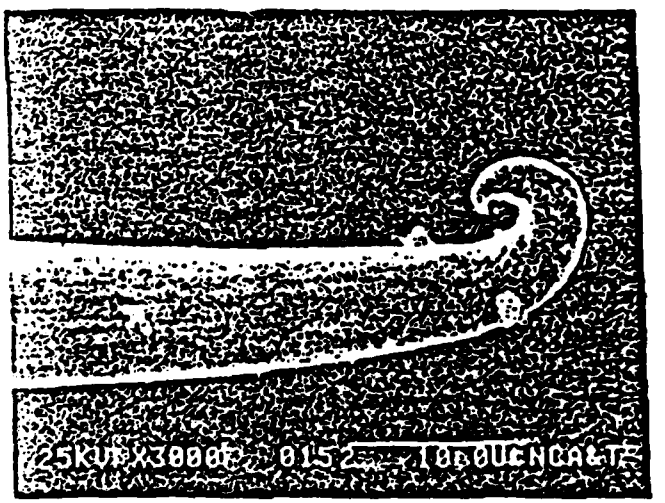

(b)

Figure 4.3. Photographs of etched tip before and after hooking. (using SEM).

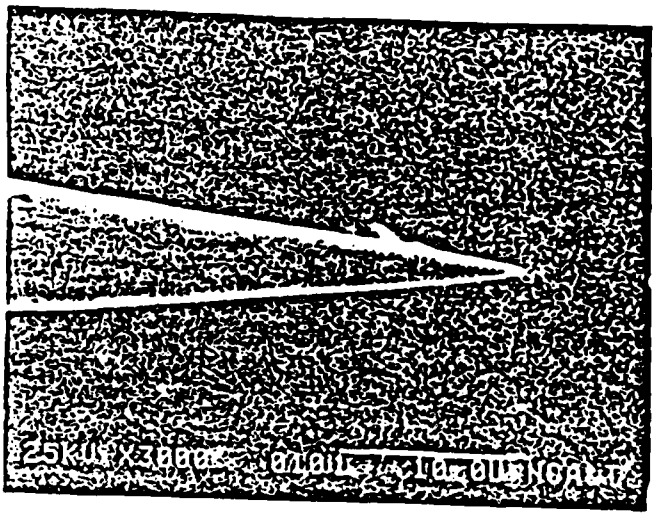

(a)

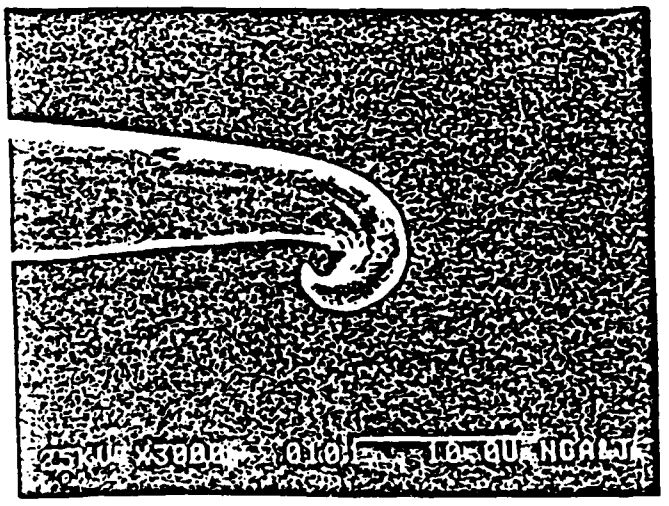

(b)

Figure 4.4. Photographs of etched tip before and after hooking (using SEM).

4.3 X-Band Detection of MIM Film Diode

Detection experiments were performed using klystrons at 8.2 GHs modulated by a variable frequency square wave. The diode mount is vibration tested by monitoring the X-band detected signal level during the test. The signal was displayed while the waveguide package was subjected to ambient vibration and severe shocks. If no noticeable changes were observed under these test conditions, the package would be shelved. The microwave setup used for detection and mixing is shown in Figure 4.5.

In the first stage of testing, a single strip Ni film was selected. the I-V curve of this film was established as shown in Figure 4.6a. This test was used to compare the earlier version of MIM film diode with the new MIM film diode design. The film was first mounted in a waveguide, stub turned and tested at X-band. An on-line commercial detector was used for comparison. The output of both detectors are shown in Figure 4.6b. The same film was used in the whisker enhanced film diode. The response is shown in Figure 4.6c. Both detected signals were stable, and as can be seen, the new MIM film diode demonstrated much higher sensitivity than the version without the whisker.

Detected X-band signals of a stabilized MIM diodes over a three week period for different film resistance are shown in Figure 4.7. The catwhiskers were taken out after each test and observed under the SEM for possible blunting. In none of the cases shown in Figure 4.7, was the tip blunted. As is clear from Figure 4.7, responses are very low for films with high ($> 10K\Omega$) or very low ($< 2\ K\Omega$) resistance.

In the mixing scheme, the two tunable X-band oscillators were set at approximately 8 GHz. The MIM film diode received radiation from these sources, caused mixing that resulted in beat signals. This signal was brought down to the KHz range by tuning the two sources and displaying the beat on the oscilloscope. Figure 4.8 shows the I-V curve of the film used in this diode and the beat from the MIM film diode and the commercial diode.

Finally, the response of MIM film diodes using the same discontinuous film but three different catwhiskers (catwhiskers with different slender ratios) was examined. The I-V curve of the film used in this experiment is shown in Figure 4.9. The catwhiskers were taken out after each test and observed under the SEM.

The SEM picture of a hooked tip and corresponding detected signal are shown in Figure 4.10. This diode was stable under severe shocks. This indicates that the sharp point has penetrated the oxide layer fully and is in electrical contact with the metal islands. Thermal cycling between 0°C and 100°C had a slight effect on diode performance. This was due to expansion or contraction of the entire whisker resulting in minute lateral movement of the bent tip on the islands. In Figure 4.11 the tip was not fully hooked, and the response was lower than that of the diode with a properly hooked tip and the signal was not stable (Fig. 4.9). Figure 4.12 showed a blunted tip and corresponding detected signal. The signal in this case is very low because the blunted tip does not penetrate the oxide layer, nor does it provide local field enhancement and a high degree of island array selectivity.

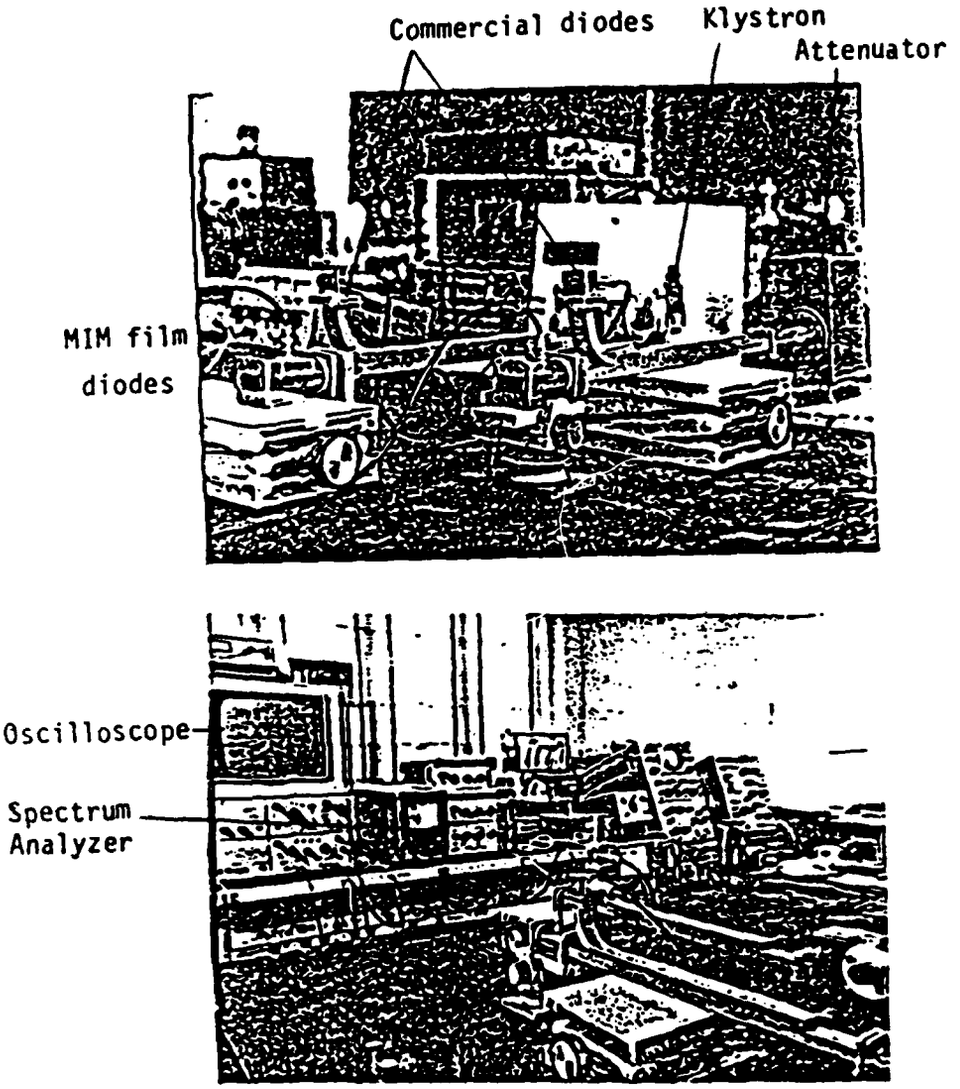

Figure 4.5. Microwave setup used for detection and mixing of the waveguide packaging diode.

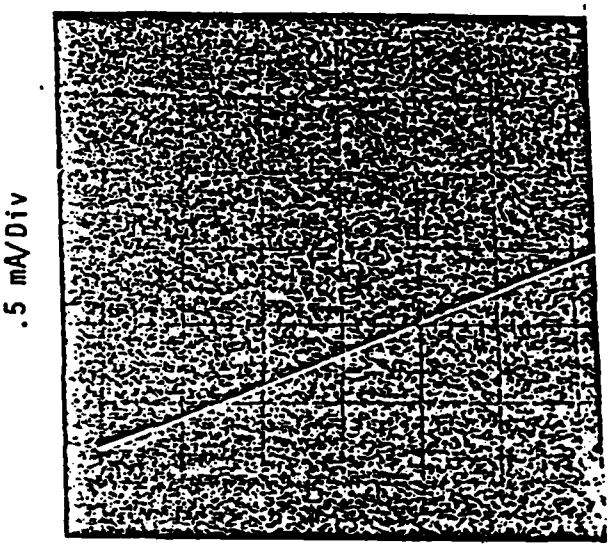

Figure 4.6a. I-V curve of the Ni film (50W, 30 sec) (R = 9KΩ) chips array and field enhanced MIM film diodes

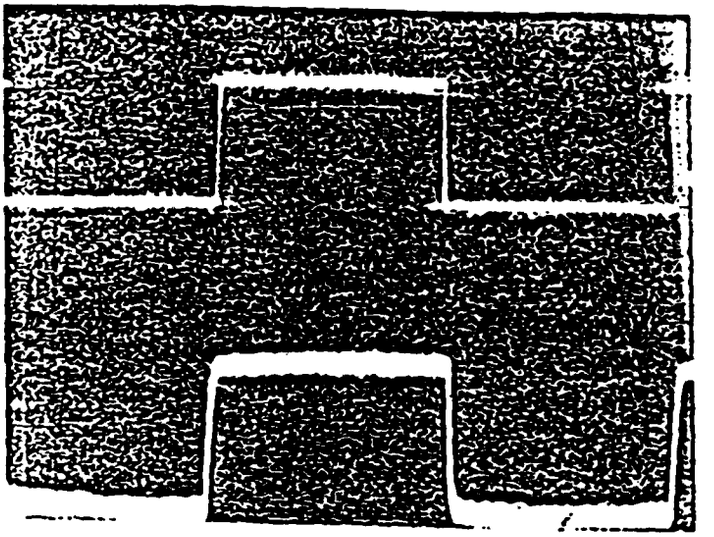

Figure 4.6b. X-band Detection of Chips Array MIM Film Diode

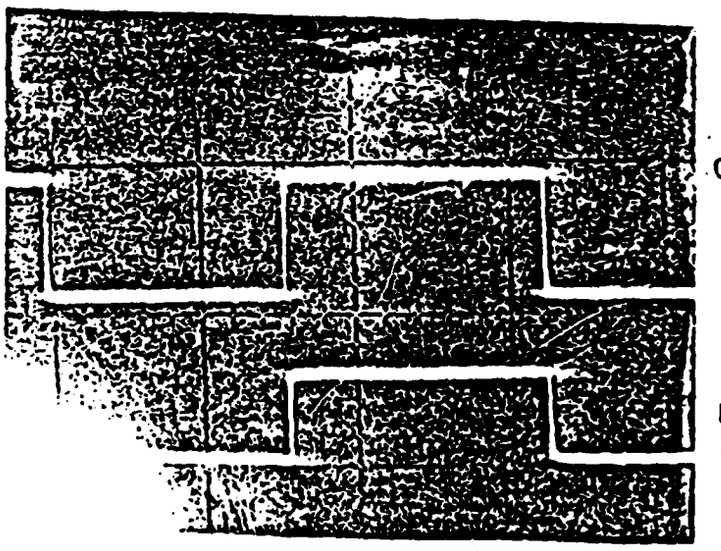

Figure 4.6c. X-band detection of field enhanced film diode

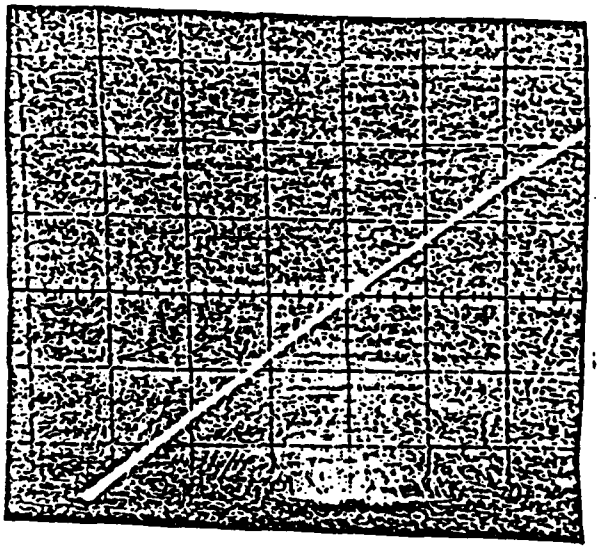

.2 mA/Djv.

1 V/Div

(i)

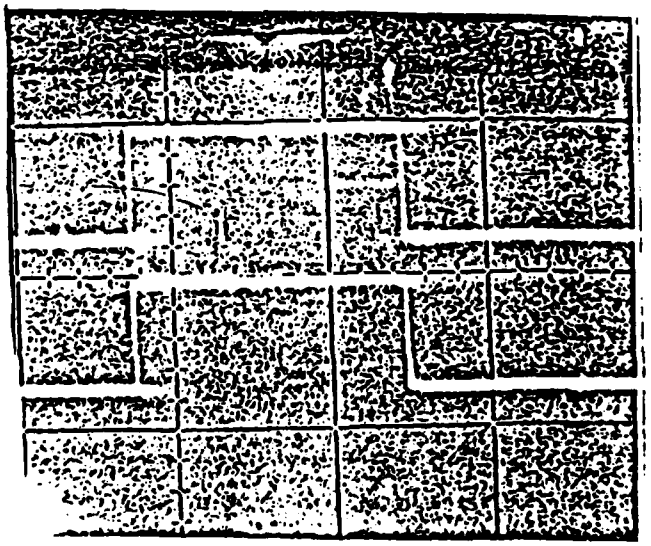

Commercial detector
2V/Div.

MIM film diode
5 mV/Div.

Time, 1 msec/Div.

Figure 4.7a. (i) I-V curve of (50 W, 30 sec) Ni film (R = 6K), (ii) and corresponding detected signal

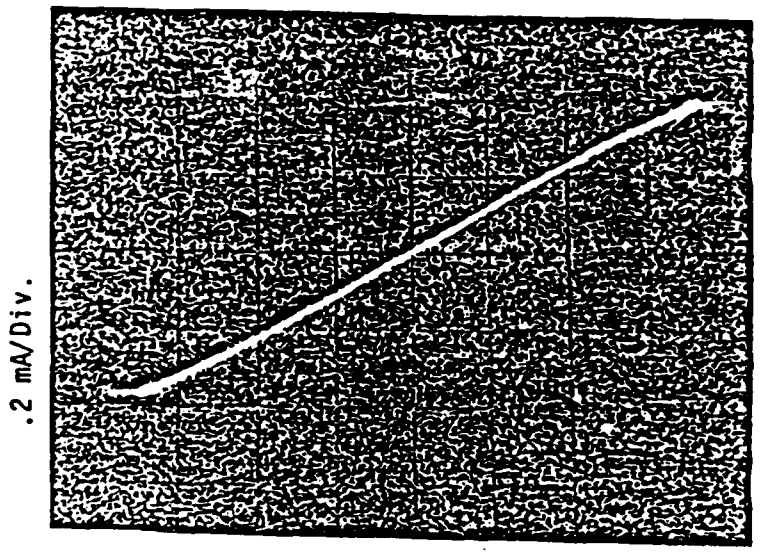

(i)

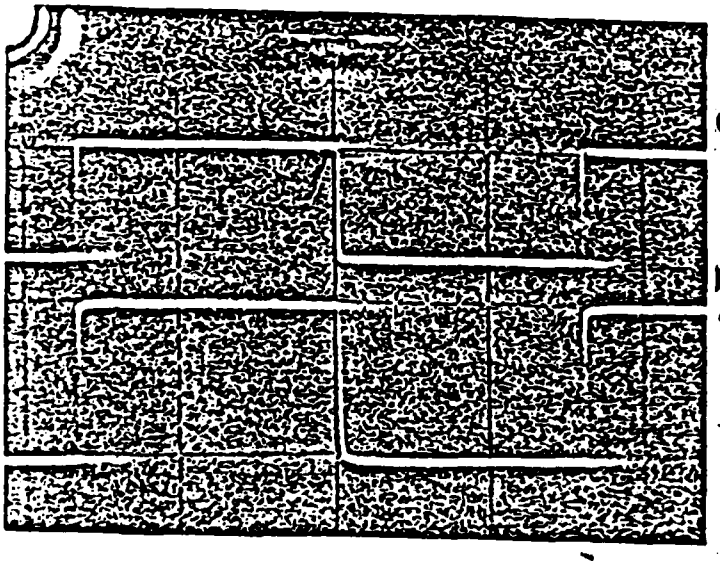

(ii)

Figure 4.7b. (i) Curve of Ni film (50 W, 30 sec) (R = 9 KΩ)
(ii) and corresponded detected signal.

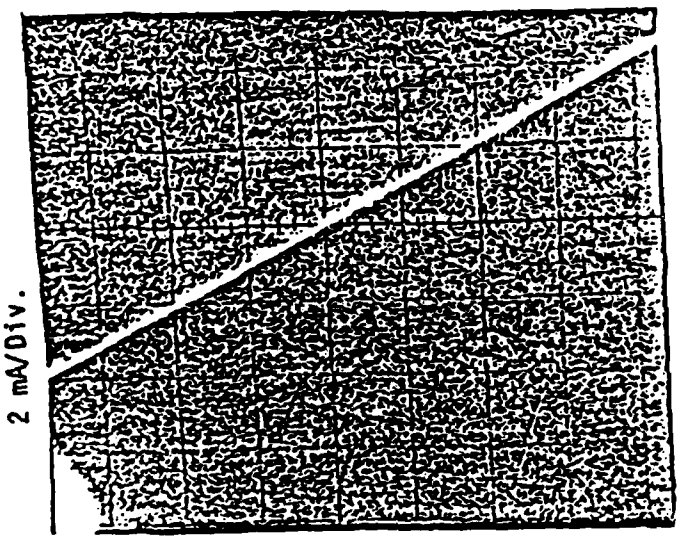

(i)

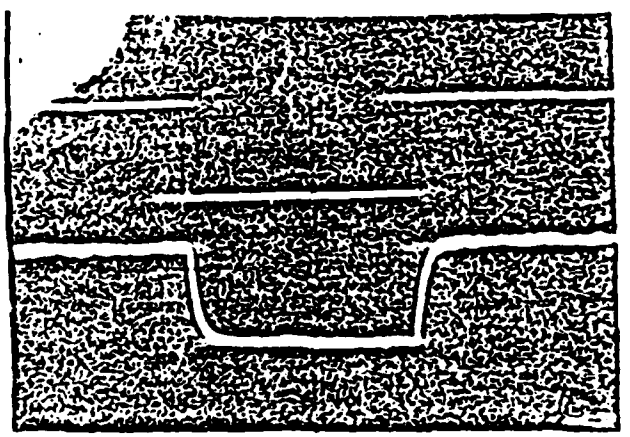

Commercial detector
2 V/ Div,

MIM film Diode
.1 mV/Div.

Time, 1 msec/Div.

Figure 4.7c. (i) I-V curve of Ni film (50W, 30 sec) (R = 14 KΩ), (ii) and corresponded detected signal

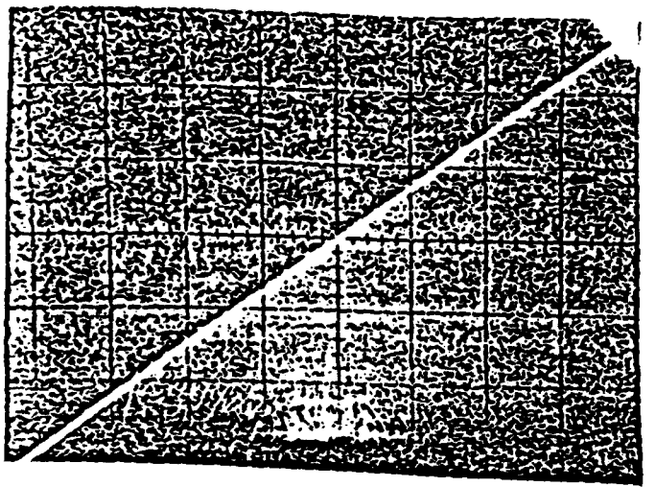

(i)

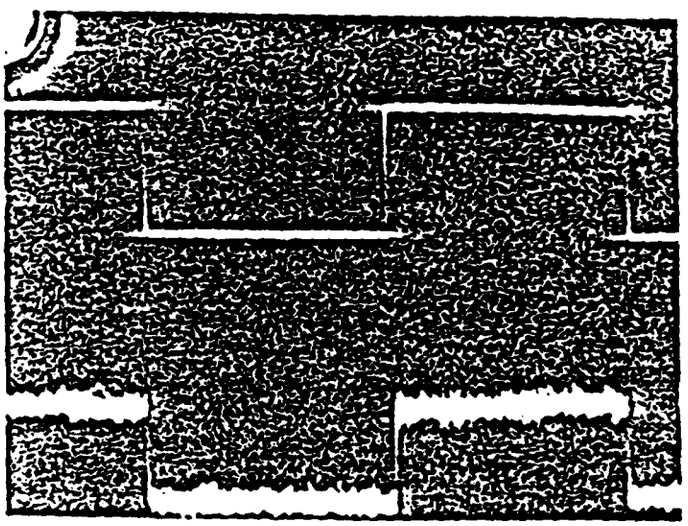

Commercial detector
2V/Div

MIM film diode
.1 mV/Div.

Time, 1 msec/Div.

Figure 4.7d. (i) I-V curve of Ni film (50W, 30 sec,) (R = 1.6 KΩ)
(ii) and corresponded detected signal.

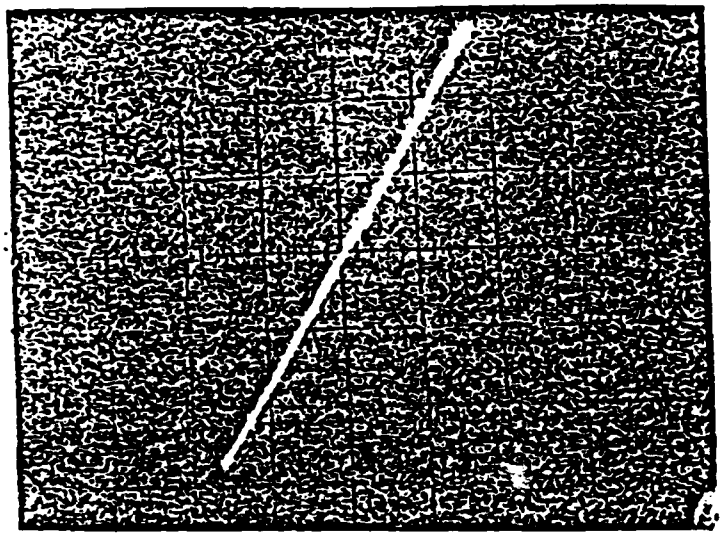

(a)

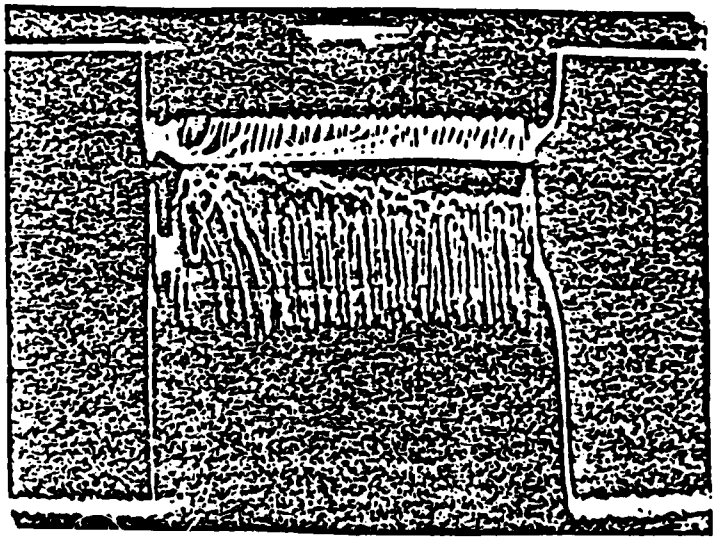

Figure 4.8 (a) I-V curve of the film (50W, 30 sec).
(b) corresponding X-band beat signal of MIM film diode and the commercial diode.

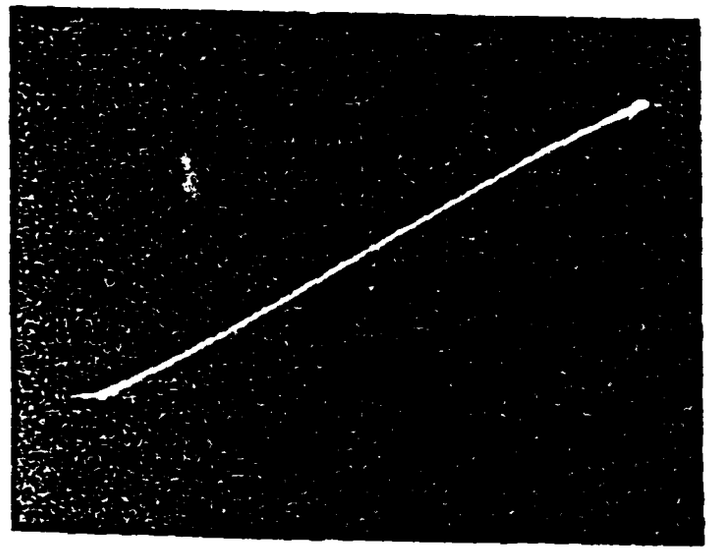

Figure 4.9 I-V curve of Ni film used in three different waveguide packaged diode with different catwhiskers (catwhiskers with different slender ratios), (see following figures).

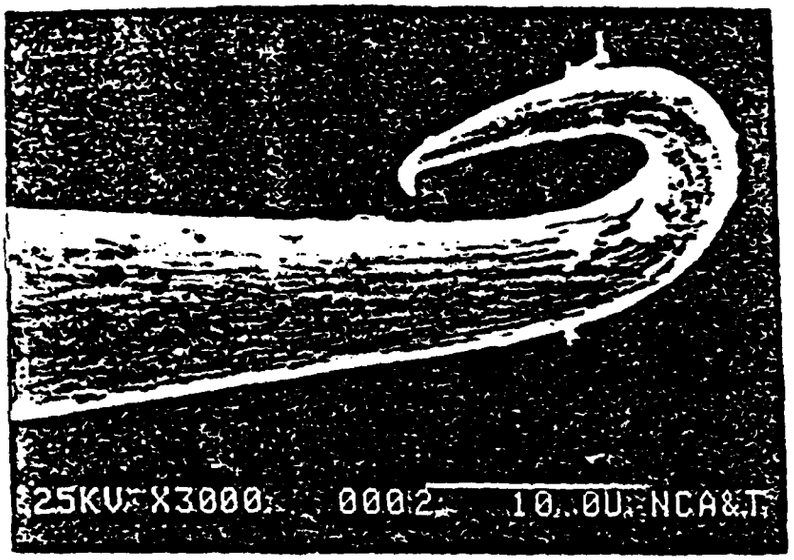

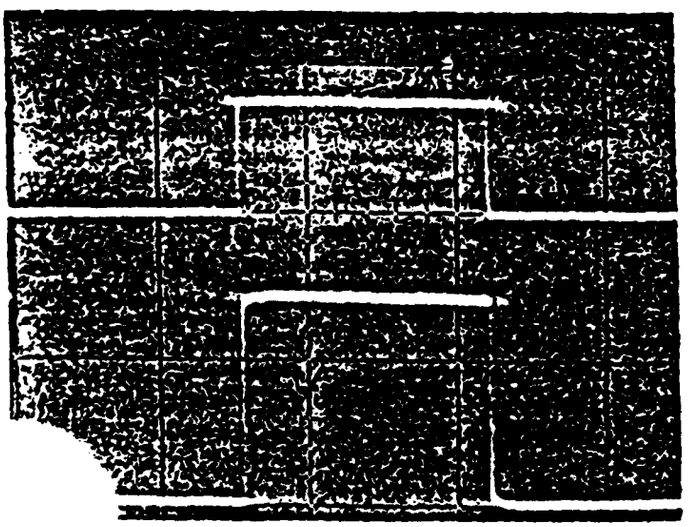

Commercial detector
2 V/Div.

MIM film diode
10 mV/Div.

Time, 1 sec/Div.

Figure 4.10. SEM photograph of a hooked tip and corresponding X-band detection of waveguide packaged MIM film diode.

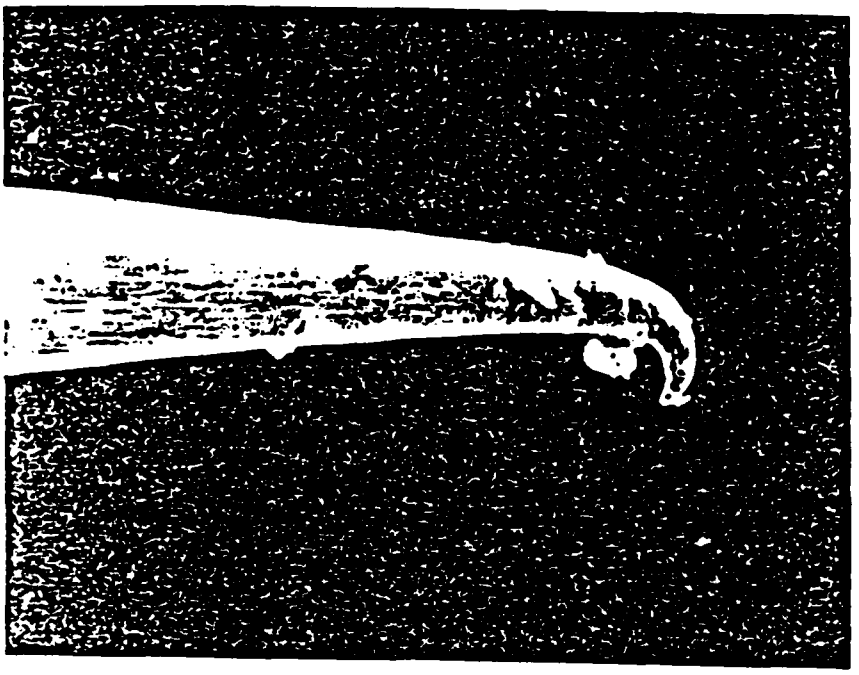

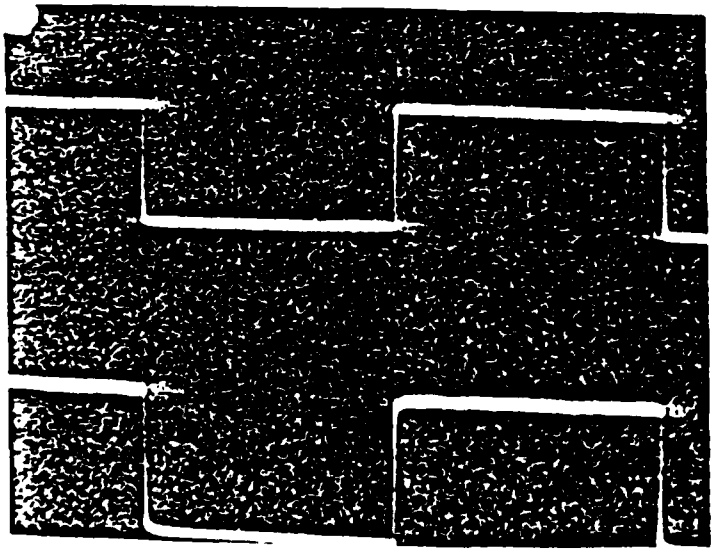

Commercial detector
2V/ Div.

MIM film diode
2mV/Div.

Time, 1msec/Div.

Figure 4.11. SEM photography of a hooked tip and corresponding X-band detection of waveguide-packaged MIM film diode.

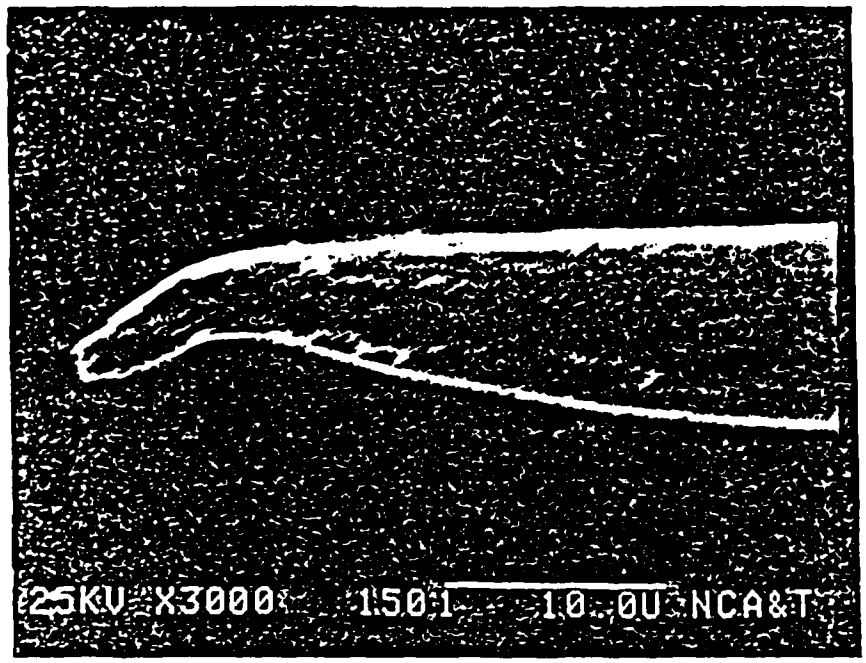

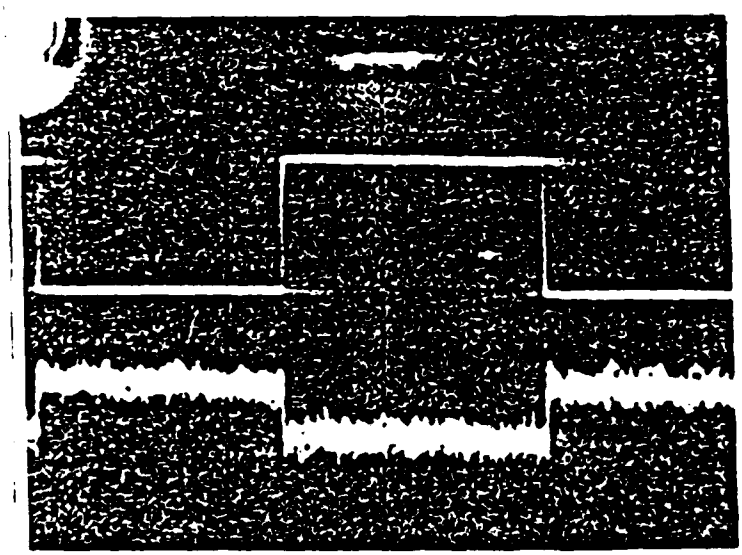

Commercial detector
2 V/Div.

MIM film diode
.2 mV/Div.

Time, 1msec/Div.

Figure 4.12. SEM photograph of a blunted tip and corresponding X-band detection of waveguide-packaged MIM film diode.

CHAPTER V

CONCLUSION

The discontinuous MIM film diodes using nickel islands have clearly demonstrated the feasibility of long term stability without severe degradation in the X-band. Its performance was comparable to the performance of the point-contact version by incorporating the tungsten whisker tip for field enhancement and array selectivity.

The planar nature of the film diode with the film and the whisker in parallel planes renders the diode immune to ambient vibrations. However, the bent tip in a vertical orientation (see Fig. 3.4) tends to move under ambient thermal fluctuations due to thermal expansion and contraction of the stem of the whisker. However, this can be removed by heat sinking the stem.

In such an MIM film diode, the sharp point has penetrated the oxide layer and is in electrical contact with the metal islands. Therefore, the tunneling region is fixed by initial film deposition, which determines interisland spacing. This feature is extremely desirable for thermal stability; while in the point contact diode, oxide layer penetration depth varies with temperature even with a hooked tip. The inherent noisy property of discontinuous film still awaits understanding and solution. This may lie in a better control of deposition for more uniform films by high resolution masking and other techniques.

REFERENCES

1. K. M. Evenson, "Frequency measurement in the optical region and the speed of light". CPEM, 1074.

2. S. Okamura, K. Ijichi, "A fast detector by discontinuous metal film for the mm through optical frequency range". Trans. Inst. Electronics Commun. Eng. Jpn., Sec. E. E60, 166 (1977).

3. K. Ijichi, S. Okamura, "A fast detector with discontinuous metal films for mm through infrared wavelengths". Electronics and Communication, Jpn. Vol. 60-C, No. 3 (1977).

4. C. Yu, S. A. Yekrangian, "Discontinous MIM film chip arrays as mm wave and infrared detector-mixer diodes". Eighth International Conference on Infrared and MM Waves. Miami Beach, Florida. December (1983).

5. C. Yu, A. Niczad, "Field Enhancement and increased island array selectivity of discontinuous MIM film diode. "Tenth International Conference on Infrared and MM Waves, Orlando, Florida. December (1985).

6. J. W. Dees, "Detection and harmonic generation in the submillimeter wavelength region". Microwave Journal. Vol. 9, p.43-56. September (1966).

7. Nishiura, Vozumi, "Electrical resistance of discontinuous metal thin films". Journal of Applied Physics. Jpn. 44, 1, p.71. (1975).

8. R. M . Hill, "Electrical conduction in Ultra Thin metal films." I. Theoretical, II. Experimental. Proc., Roy. Soc. AA-309, p.377, (1969).

9. S. Miyake, "Fundamental thin-film technology". A. Shoten, p.40 (1968). From C. A. Neugebauer: Measurement Techniques for Thin Films, p.191, Electrochem. Soc. (1967).

10. S. A. Schelkunoff, Advanced Antenna Theory, John Wiley & Sons, (1955).

11. S. A. Schelkunoff, Antenna Theory and Practice, John Wiley & Sons, (1952).

12. E. A. Wolff, Antenna Analysis Wiley, New York, (1966).

13. J. C. Kraus, Antenna, John Wiley & Sons (1966).

14. C. Yu, M. A. Hemmatian, A. Niczad, Y. Taghipoor, A. Yekrangian, "A Systematic study of the effect of hooking upon contact on the performance of electrolytically etched point contact MOM diodes". SPIE Technical Symposium East/85, Arlington, VA April (1985).

15. T. E. Sullivan and P. H. Cutler, "The use of Antenna theory to calculate the electric field emission metal whisker diode". Surface Science, 62, (1977), p.455-471.

16. J. G. Simmons, "Potential barrier and emission - limited current flow between closely spaced parallel metal electrodes". Journal of Applied Physics, Vol. 35, August (1964).

17. D. Bohm, Quantum Theory, Prentice-Hall, Inc. Englewood Cliffs, New Jersey, (1959), p.275.

18. P. Frayn, N. Chandlen, M. Botton, "Point-contact diode submillimeter detectors". Appl. Phys., Vol. 11, (1978).

19. H. D. Riccius, "Improved Metal-Insulator-Metal point-contact diodes for harmonic generation and mixing". Applied. Phys., 17, 49, Vol. 52, 1978.

20. J. W. Dees, "Detection and harmonic generation in the submillimeter wavelength region". Microwave Journal, Vol. 9, p.48-55, September (1966).

21. M. McColl, "Review of submillimeter-wave mixers". Proceeding of Society of photo optical instrumentation engineers, Vol. 105 p.24-34, (1977).

22. K. M. Baird, "Frequency measurements of optical radiation". Physics Today, January (1983), p.52-57.

23. B. Twe, S. E. Schwarz, "Properties of infrared catwhisker antennas near 10.6μm". Applied Physics Letter, Vol. 26, No. 12, 15, June (1975).

24. E. Wiesedanger, F. Knewbuhi, "Thin film MOM diodes for infrared detection". Applied Physics. 13 pp. 343-349. (1977).

25. C. Yu, M. A. Hemmatian, " Stability parameters of stable hooked-tip MOM point contact diode as mm wave and infrared detector-mixer". Eight International Conference on Infrared and MM Waves. Miami Beach, Florida. December (1983).

26. C. Yu, M. A. Hemmatian, A. Yekrangian, "Mounting improvements of the MOM point contact diode". Tenth International Conference on Infrared and MM Waves. Orlando, Florida December (1985).

27. B. J. Clifton, IEEE Trans. MIT 25,457 (1977).

28. S. A. Yekrangian, "Fabrication and testing of discontinuous metal film diodes as microwave and mm wave detector mixer". North Carolina A&T State University, Thesis, May, (1986).

A Reprint from the

PROCEEDINGS

Of SPIE-The International Society for Optical Engineering

Volume 544

Millimeter Wave Technology III

April 9-10, 1985
Arlington, Virginia

A systematic study of the effect of hooking upon contact on the performance of electrolytically etched point contact MOM diodes

C. Yu, M. A. Hemmatian, A. Niczad, Y. Taghipoor
Electrical Engineering Department, North Carolina A&T State University
Greensboro, North Carolina 27411

A. Yekrangian
Electrical Engineering Department, Howard University, Washington, D.C. 20059

A systematic study of the effect of hooking upon contact on the performance of electrolytically etched point contact MOM diodes

C. Yu, M. A. Hemmatian, A. Niczad and Y. Taghipoor

Electrical Engineering Department, North Carolina A&T State University
Greensboro, North Carolina 27411

A. Yekrangian

Electrical Engineering Department, Howard University, Washington, D.C. 20059

Abstract

To resolve the controversy regarding hooking of the whisker tip without damage as a reliable method for stabilizing the MOM point contact diode without significant degradatio of diode performance, a systematic study is implemented to control the fabrication of such tips, the contacting process and monitoring of diode performance in the microwave and mm wave region.

The fabrication and contacting processes are monitored by microscopes, and the tip with and without hooking is scrutinized with the SEM. Results so far have indicated the reproducibility of the etching process, and the tolerance range of tip dimensions that will mak contacting process and surface less critical. Improvement in stability is also significa with controlled hooking of the tip with no noticeable loss of diode sensitivity. The stability is long term and is quite immune to moderate vibrations and laser heating. Diod performance is monitored at 10 and 50 GHz in direct detection and mixing both before and after hooking.

Introduction

As a follow-up on our work on the stability of hooked-tip MOM point contact diodes reported previously[1], we will present our current results on the fabrication and control o the etching and hooking parameters of the whisker tip. This is a systematic study that involves a painstaking procedure to attempt to achieve reproducibility of the etched tip with the optimum slender ratio, what we call the reproducibility indicator; and a hooking procedure that can serve as the diode stability indicator.

Electrolytic etching process standardization

A 3N KOH solution, freshly prepared was used for each tip etching so as to maintain the etching solution at constant strength. Electrode spacing with the tip to be etched serving as one electrode was also kept fixed for all tip etchings. An 8V ac was applied directly to the electrodes, with precautions taken to reduce circuit resistance to a minimum of 1-2 ohms. Circuit resistance variation due to the introduction of metering or poor contact between the tungsten wire to be etched and the vice that held the wire in a firm grip was often reflected in significant variation in the etching time. Once these parameters were established and held constant, the shape of the etched tip was then solely controlled by the depth of immersion of the wire in the electrolytic solution. Miniscus etching determined the tip shape, with modification dependent critically on the time required to etch the immersed portion of the tungsten wire. Three typical etched-tips for three different immersion depths are shown in Fig. 1, at two magnification settings of the SEM. The portions of the wires with horizontal striations are the unetched part (see Fig2 pictures with 540x magnification); the 3000x level of magnification is used to study in detail the etched portion of the wires. The shape of the etched portions determine critically the amount of hooking and the type of hooking possible when the tip comes in contact with the nickel post and penetrates into the surface oxide layer.

The reproducibility indicator-undamaged-hooked studies

Control of the etching parameters has resulted in the fabrication of whisker tips of reproducible shapes. Interest was then focussed on the optimum tip shape and its reproducibility. A reproducibility indicator was established for a tip with an optimum shape defined as that which led an optimum undamaged hook. The hooking process was thus designated as the means to establish this indicator.

Figure 1a presents an etched tip, resulting from a shorter than optimal length of wire immersed in the KOH solution. The tip was not sufficiently slender, so that upon contact with the nickel post, no hooking was possible. With increasing contact pressure,

tip blunting eventually occurred. This is defined as a damaged or blunted tip. Such an MOM diode exhibited totally unsatisfactory detection performance when tested at 10 GHz. Figures 2a, b, c, demonstrate tips in the range of the optimum shape as verified by the proper amount of hooking without tip blunting or damage, as seen in Figs. 2aa, bb, cc.

This optimum tip shape was achieved by increasing the immersion depth of the tungsten wire in solution. An optimum hook is one that possesses an undamaged tip very close to the elbow of the hook, where contact with the oxide layer occurs. The proximity of the sharp tip to the elbow is essential in preserving diode performance under hooking. The sharp tip is known to enhance the electric field which should best take place near or at the MOM junction area. Detection performance of the MOM diode with this hooked tip was as good as that of an unhooked tip; stability of this diode was observed to be long term.

Increasing wire immersion in solution by another 30% led to a very slender tip, as shown in Fig. 3a. As evidenced in Fig. 3aa, the actual whisker tip would always produce a hook similar to the optimum. However, with slight increase in contact pressure, the shaft of the tip gave way, producing a large arch with an elbow now very distant from the actual hook. This elbow was the MOM junction area, where tunneling was pressumed to take place. The tunneling process in this case did not receive sharp-tip field enhancement. Detection performance of such a diode was poor, and so was the stability due to the lack of spring action of this large arch.

After prolonged and extensive testing for the optimum hooked tip, and having arrived at the appropriate etching parameters, it is natural to establish the range of these parameters in which the optimum tip shape could be maintained without degradation in both detection and stability. Tips were repeatedly fabricated under these optimum parameters and examined in detail under the SEM. The results are shown in Figs. 3bb and cc. They show tips made under presumably identical conditions to possess slender ratios that are almost identical. This is further verified by the reproducibility indicator, that is, the hook formation. However, elbow formation varies significantly.

Other etching conditions

Whiskers were also etched with the application of a dc voltage of the same magnitude as that used in ac etching. At optimum immersion depth of the tungsten wire, the resulting etched tip was dramatically different from the ac etched optimum tips, as demonstrated in Fig. 4. Extremely short tips appeared that could not be hooked at all. One possible cause for such a discrepancy may lie in the chemical behavior of the KOH solution in dc conduction mechanisms between ac and dc etching.

Nickel post studies

Commercially drawn nickel wires were not used as the post in the MOM diode structure due to the fact that the nickel surface on which a natural oxide layer will be formed is usually very coarse, similar to the tungsten wire surfaces with severe striations. The contacting process was greatly improved and standardized with the use of a quartz cylinder at the ends of which a nickel film was sputtered. With this process, the nickel layer thickness could be controlled by controlling the sputtering time or sputtering power, and the nickel surface was guaranteed to be smooth. Oxide layer was then uniform on the nickel post. Of course, the quartz post had a very small thermal expansion coefficient, so that MOM junction diode width hardly varied with ambient temperature. Nickel film deposited was examined by the SEM; film uniformity was acceptable as seen in Fig. 5 under 5400x magnification. The granular nature of the film is still evident, although the film is electrically continuous. Attempts are underway to improve film quality by reducing the granular characteristics.

Waveguide mounting

A program is in process for the design of waveguide mounting of the point contact MOM diode. An initial model has been built and is shown in schematic in Fig. 6. Detection at microwave frequency was achieved, but stability of the diode was poor, due mostly to a mounting problem using a micrometer stage. This is expected to be minor.

Conclusions

The results of a systematic study of the reproducibility and stability of the electrolytically etched MOM point contact diode with an undamaged hook have demonstrated the feasibility of such a configuration. Control of the etching parameters and the diode mount have shed some light on the feasibility of commercial manufacture of such a device. In this case, tighter control of etching parameters is essential.

Acknowledgements

The authors wish to thank Ms. Dora Liverman of the Biology Department for assistance in the SEM work. This research is performed under Navy Contract No. N00014-83-K-0569 and Army contract No. DAAG 29-83-G-0114.

References

1. C. Yu, and M. A. Hemmatian, "Stability Parameters of Stable-Hooked-Tip MOM Point Contact Diodes as MM Wave and Infrared Detector-Mixer", Proc. 8th Intern. Conf. on Infrared and MM waves. T6.4, Dec. 12-17, 1983.

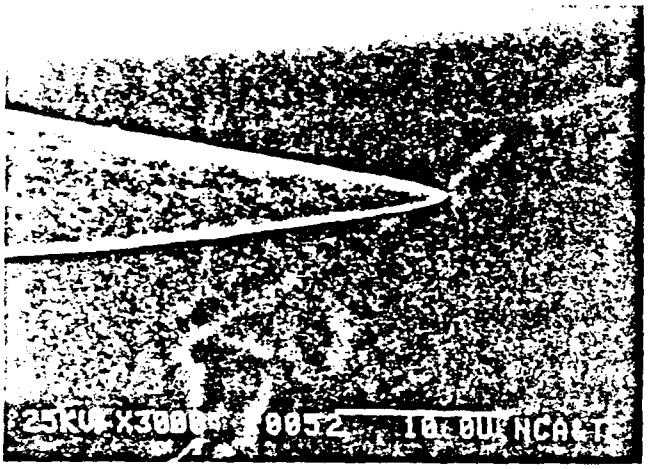
25KV X3000 0052 10.0U NCA&T


25KV X3000 0052 10.0U NCA&T

Figure 13a.

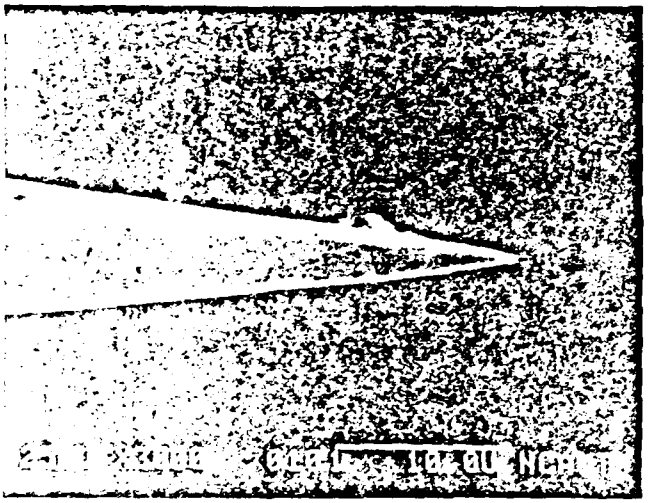

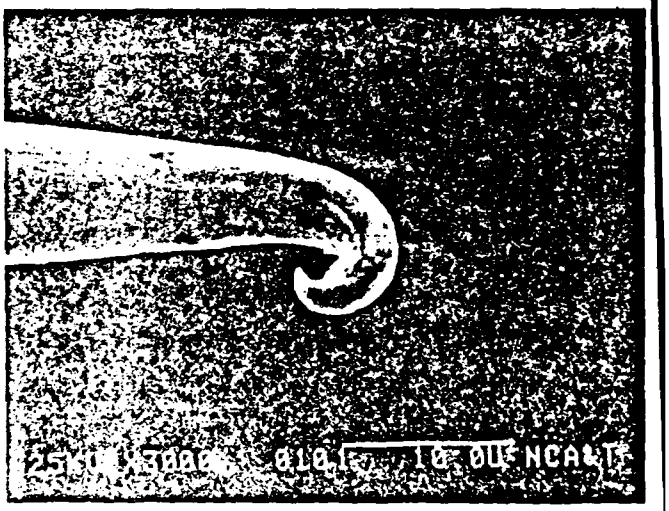
25KV X3000 0102 10.0U NCA&T

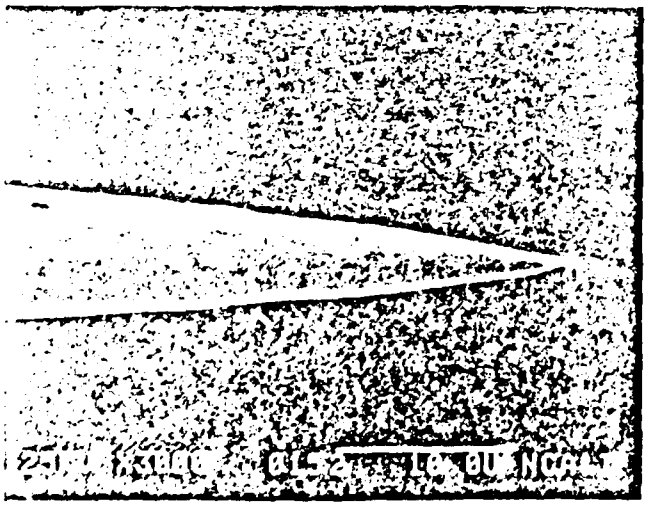

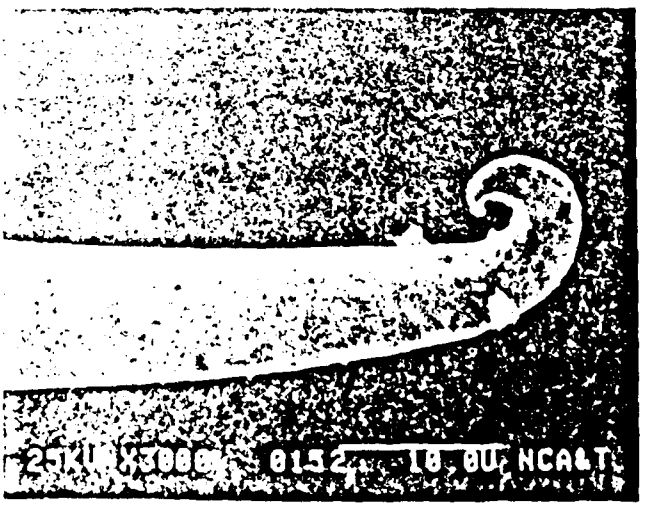
25KV X3000 0152 10.0U NCA&T

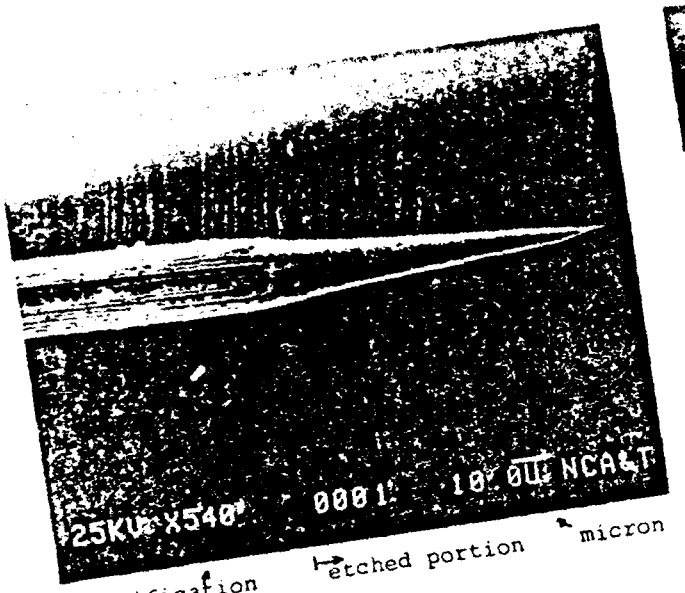

Magnification ↦ etched portion ↖ micron

Figure 2a

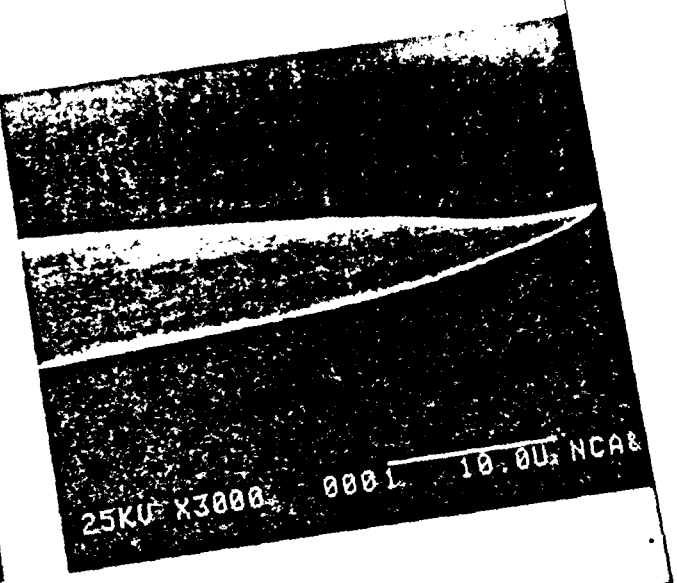

Figure 2aa

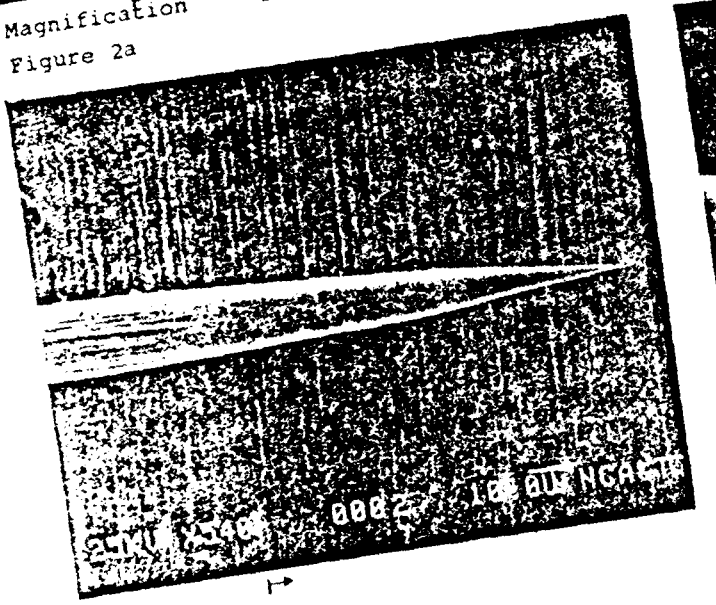

Figure 2b

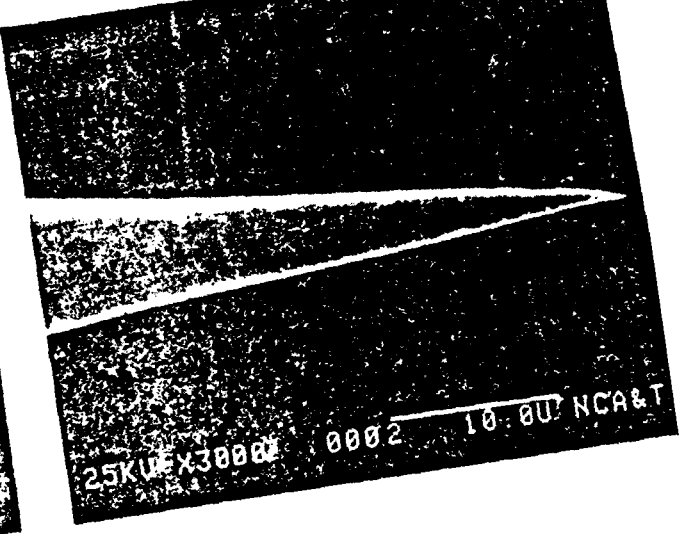

Figure 2bb

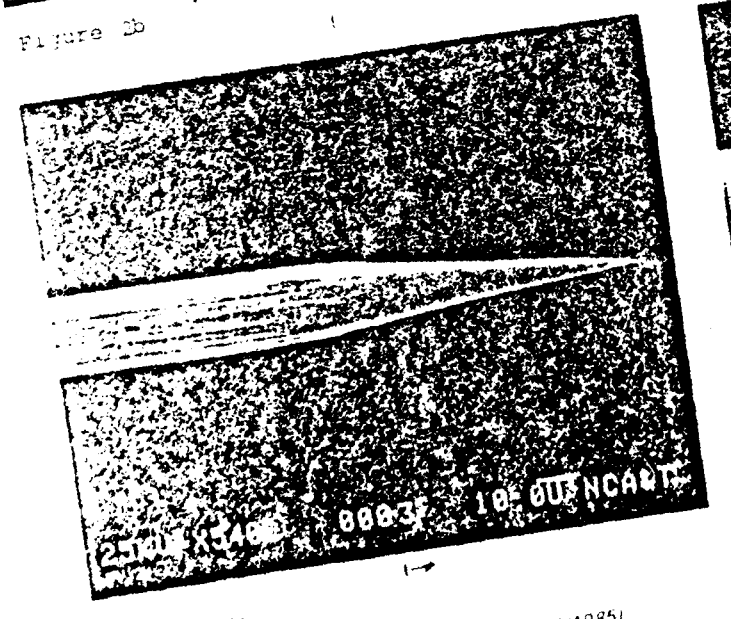

Figure 2c

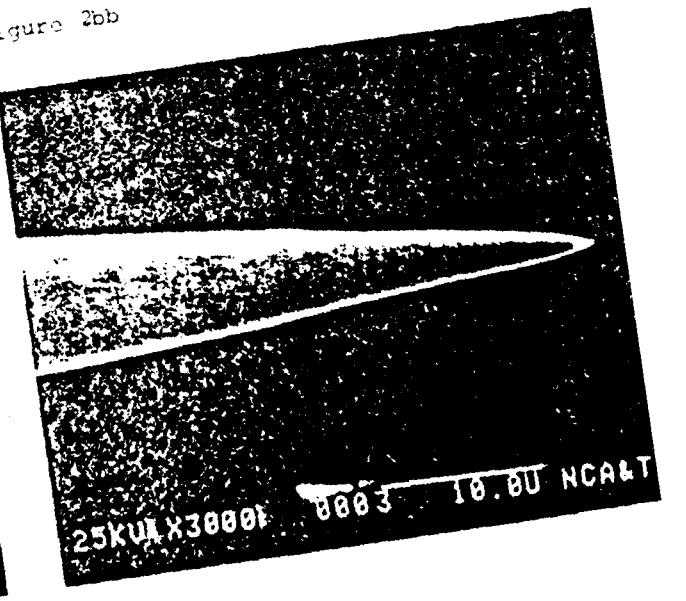

Figure 2cc

Figure 2

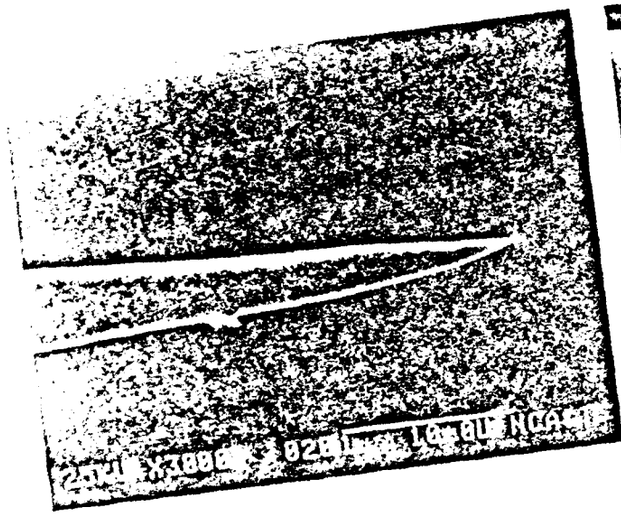

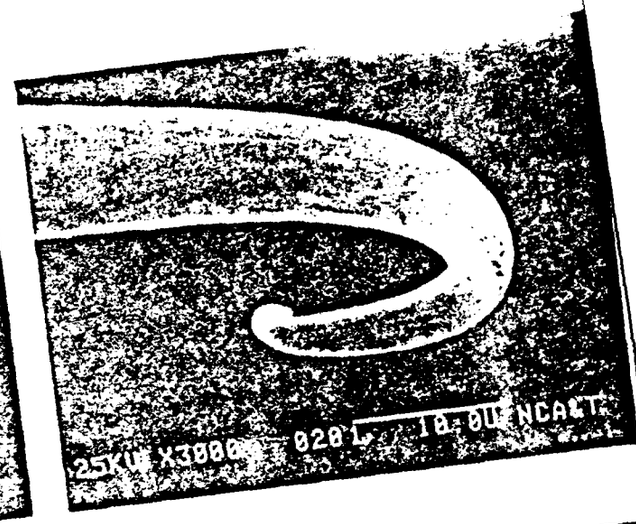

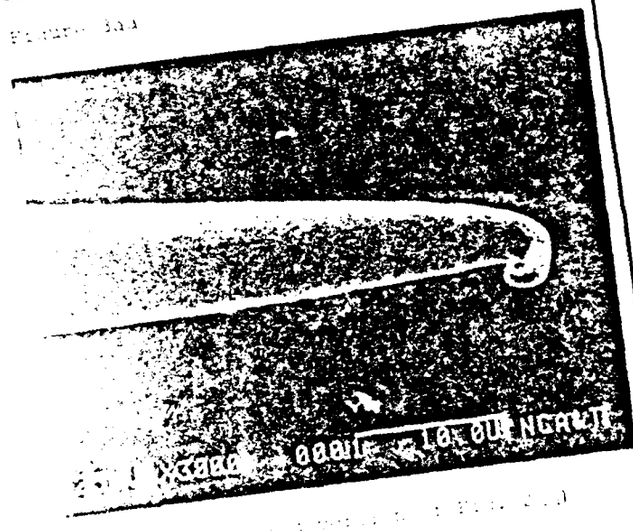

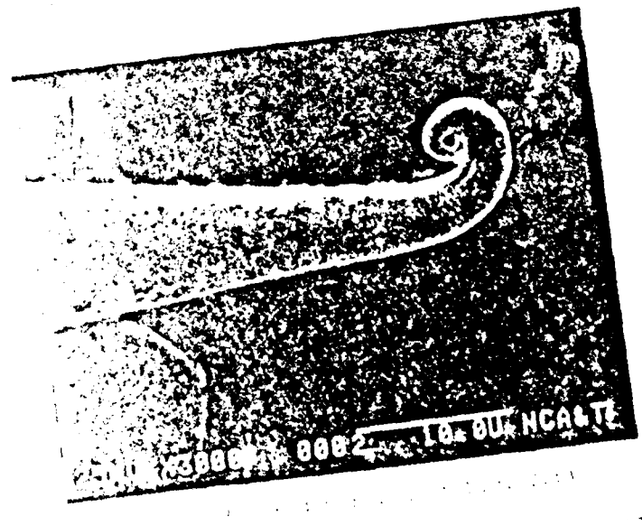

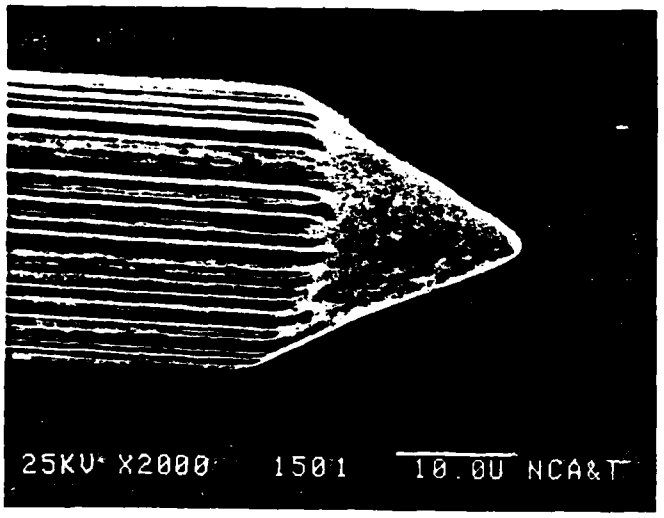

Figure 4.

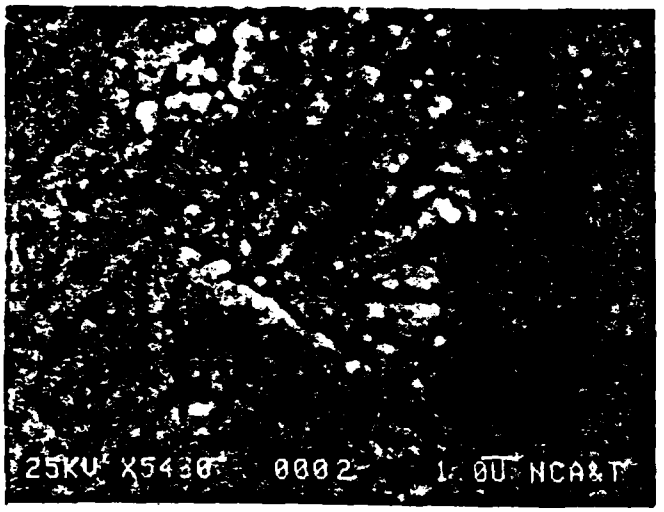

Figure 5

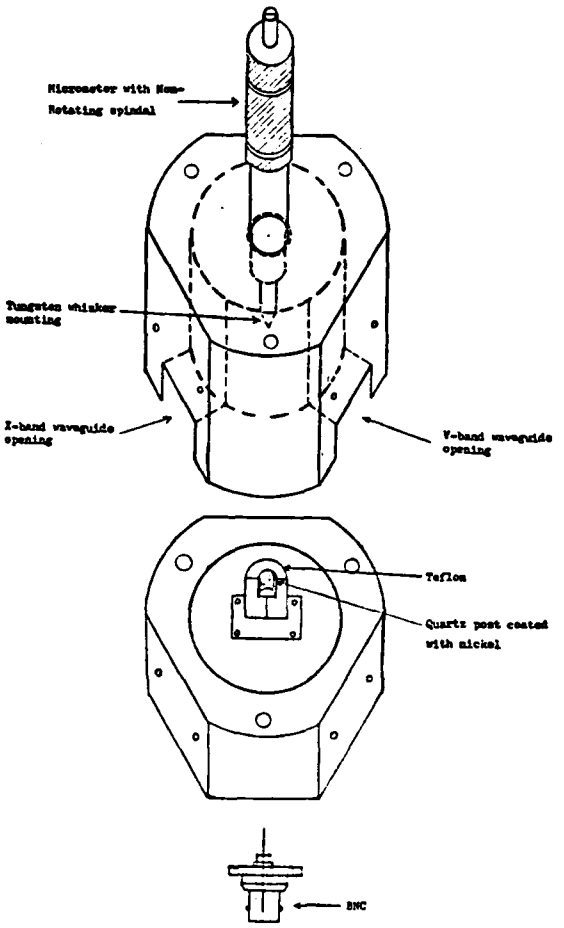

Isometric drawing of MOM point contact diode packaging.

Figure 6.

MOUNTING IMPROVEMENTS OF THE MOM POINT CONTACT DIODE

C. Yu, M. Hemmatian and A. Yekrangian

Electrical Engineering Department
North Carolina A & T State University
Greensboro, NC 27411

ABSTRACT

A planar mounting structure is devised that renders the etched tungsten whisker and the nickel post one integral mechanical structure with possible orders of magnitude improvement in the mechanical stability of the hooked-tip MOM point contact diode. Experimental results are presented.

INTRODUCTION

Success of improving the mechanical, electrical and thermal stability of the metal-oxide-metal point contact diode by deliberately hooking an appropriately etched tungsten whisker tip without blunting has been reported by us[1]. To prevent degradation in responsivity, hooking must not be excessive, and this,as is known[2], cannot render the device totally immune to severe ambient mechanical and thermal disturbances. Our current efforts are directed at the refinement of the hooked-tip mounting structure.

OBJECTIVE

The conventional free standing whisker, either in a vertical or horizontal arrangement is obviously extremely vulnerable to vibrations. It is the thought of anchoring the whisker in some fashion that leads to the idea of making the whisker and nickel post one integral structure. It is hoped that this configuration will remove most of the relative motion between the tip and the post, thus the major portion of the mechanical instability of the diode; then the hooked tip with its inherent spring action and the free etched tip pointing away from the junction area should be able to accommodate residual mechanical vibrations. The hooked tip has always been capable of handling extensive thermal fluctuations either due to the ambient or when illuminated by intense laser radiation in laser detection and heterodyne applications.

NEW DIODE DESIGN

The essence of the new diode mount lies in the integration of etched tungsten whisker and the nickel post into a single mechanical structure. The X band is chosen for diode testing since waveguide packaging of the diode mount is convenient due to reasonably large dimensions. A nickel coated quartz cylinder with ends polished serves as the nickel post to assure negligible thermal expansion of the post. It is then directly silver cemented to the inside broad face of the X band waveguide. The etched tungsten whisker is also silver cemented onto a quartz plate with the etched tip protruding over the edge of the plate. The latter is thus used as a mobile carriage both for insulating the whisker electrically from the grounded waveguide, and thus the nickel post, and also for transporting the whisker towards contact with the nickel post. The carriage must have a tight fit with the broad dimension of the waveguide to minimize play of the carriage during sliding. The tip and post are so positioned that when the carriage is within range, the protruding whisker tip lands approximately centrally on the end face of the nickel post. The carriage is held securely by a translation stage, which provides micron scale movement for the protruding tip along the common axis of the whisker tip and the nickel post. A small amount of glue is applied underneath the carriage for eventual securing and integration of the carriage to the waveguide, making the whisker and post one integral structure. The glue is sufficiently slow setting, so that there is ample time for maneuvering to achieve optimum penetration of the etched tip into the nickel surface oxide layer. This optimum is established via X band detection. This position is then held until the glue sets. The signal is tapped from a BNC jack mounted on the top face of the waveguide (see Fig. 1). It is important that etched tips of optimum slenderness be used for a controlled, undamaged hook. Such tips are identified by SEM examination, and only those of closely mathcing shapes are selected (Fig. 2).

DIODE TESTING

VIBRATION TEST. X band detection scheme is used to monitor this test. The signal detected by the MOM diode is displayed while the waveguide packaged diode is subject to ambiont vibrations. Severe shocks are also administered to the diode package. If no noticeable changes are observed under these test conditions, then the package is shelved. The same set of tests is performed daily on the package over a period of weeks to discover any aging effects.

THERMAL CYCLING TEST. A mechanically stabilized and properly aged diode package is placed in an environment, where the temperature can be varied from dry ice to boiling temperatures. After such ther-

CH2204-6/85/0000-0133 $01.00 © 1985 IEEE

mal cycling , the diode package is tested at X band for possible degradation in responsivity. Such tests are also conducted during thermal cycling.

Control measures are used in the fabrication of the etched tip so that tips of nearly identical shapes are used as judged from SEM pictures. Three waveguide packages are made for repeatability tests. These packages will not be disassembled for continuing aging tests.

TEST DATA

The diode packages are found to be orders of magnitude more stable than previous structures, where the tungsten whisker tip and the nickel post are physically seperate. Slight variations during thermal cycling may be due possibly to the fact that oxide layer penetration by the tip at room temperature is not optimum. At optimum oxide depth, responsivity reaches a flat top where it is least sensitive to thermally induced depth variations[2].

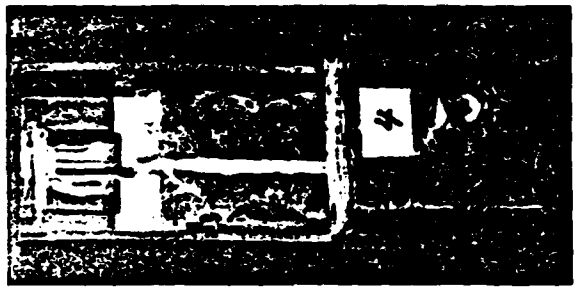

Fig. 1. Waveguide packaging of diode.

CONCLUSIONS

The integral structure of the diode mount has been demonstrated to have the capability of removing the major portion of the vulnerability of the point contact diode to mechanical vibrations. The use of quartz as the post and carriage material together with proper hooking of the tip have contributed significantly to the high degree of immunity of the diode structure to thermal effects, whether be it external ambient or irradiation by laser radiation.

The next stage of our work will involve further miniaturization of the package for mm wave and laser frequency applications.

Acknowledgements: This research is performed under Navy Contract N00014-83-K-0569 and Army Research Office Contract DAAG 29-83-C-0114.

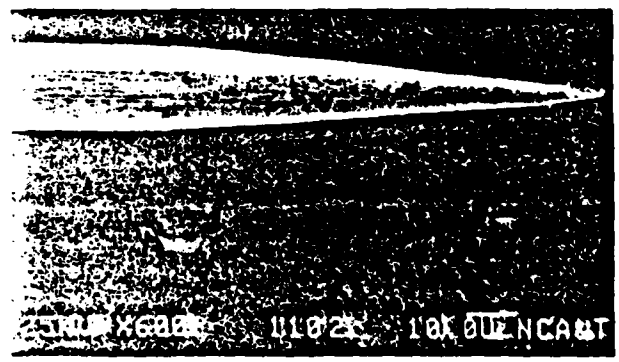

Fig. 2. SEM pictures of etched tungsten tips of nearly identical shape.

REFERENCES

1. C. Yu, M. Hermatian, A. Niczad, Y. Taghipour, and S. A. Yekrangian, "A Systematic Study of the Effect of Hooking Upon Contact on the Performance of Electrolytically Etched MOM Point Contact Diodes", SPIE Technical Symposium East/85, April 8-12, 1985, Arlington, Virginia.
2. Bor-long Twu, and S. E. Schwarz, Appl. Phys. Lett. 25, No. 10, 595 (1974).

Y. Yasuoka, T. Sakurada, and T. Miyata, Jap. J. Appl. Phys. 17, 171 (1978).

FIELD ENHANCEMENT AND INCREASED ISLAND ARRAY SELECTIVITY OF THE DISCONTINUOUS MIM FILM DIODE

C. Yu and A. Niczad

Electrical Engineering Department

North Carolina A & T State University
Greensboro, NC 27411

ABSTRACT

The receiving properties of the discontinuous metal-insulator-metal film diode are significantly improved by the incorporation of the tungsten whisker antenna that enhances the incident field strength over selected metal island arrays for optimum conduction paths. The planar version is also mechanically stable.

INTRODUCTION

As an alternative to the metal-oxide metal point contact diode, we have designed and tested a planar version using discontinuous nickel films[1] vacuum deposited onto a glass substrate. As previously reported[2] , our success so far with this diode is in the assurance of stability, while the introduction of IC chip arrays is met with limited success in improving the responsivity by increasing the area of exposure to radiation. However, due to the highly unpredictable and uncontrollable properties of each chip, their interconnection often leads to adverse results.

Having worked extensively on the point contact MOM diode[3] , our understanding of the local field enhancement by a sharp point, prompted us to design a hybrid structure that utilizes the planar feature of the film deposition on a planar glass plate for stability and the reintroduction of the etched whisker tip used in the point contact diode in contact with the island arrays for array selection and local field enhancement.

OBJECTIVE

It is our aim to design and test a hybrid planar diode package consisting of discontinuous nickel film with islands seperated by naturally grown oxide layer where tunneling occurs in contact with anetched tungsten whisker tip. The diode structure is then packaged in X band waveguide and tested for stability and improvement in responsivity.

NEW DIODE DESIGN

Nickel film deposition on glass substrate (1)follows the same procedure as reported previously [1] . The metal island arrays are probed for resistance values in the range of less than 10 KOhm. This is the range of high island density, hence narrow oxide layer between islands, thus high tunneling probability. Desirable film patches are removed with their glass substrates intact, and glued onto another glass plate (2). The etched tungsten whisker is laid flat and silver cemented to glass plate (2) with the slightly bent tip positioned such that it will be in strong contact with the metal film patch on glass plate (1). The difference in the vertical elevations of the two plates, which may also be made to vary, leads to variable contact pressure the tip can exert on the film. This contact pressure can also be controlled by controlling the shape or slenderness of the tip, which in turn controls the amount of hooking upon contact. This technique is very familiar to us through our experience with the MOM point contact diode. The diode mount is then installed in the X band waveguide for packaging and testing (see Fig. 1).

TEST PROCEDURE

The diodes are tested for responsivity at X band. The question of stability of the diode structure arises since the whisker tip is again employed. The nature of the film is readily probed through the I-V characteristic of the diode, and its degree of nonlinearity. Excessively high diode resistance is an indication of the large seperation between islands, and hence poor performance. Excessively low diode resistance is clearly a sign of the progressively continuous nature of the film.

The sharp tip is used for local field enhancement and island array selection. It is thus expected to penetrate the nickel oxide layer completely and make good electrical contact with the islands. Tunneling occurs between islands, where the oxide layer thickness is fixed. In the process of penetration, the tip is always either hooked or blunted, depending on the slenderness of the tip.

This type of diode structure is subjected to ambient vibrations and shocks. Waveguide packaged diodes are also shelved for aging studies.

TEST DATA

As in the case of the MOM point contact diode, hooking of the whisker tip does not degrade the responsivity

CH2204-6/85/0000-0135 $01.00 © 1985 IEEE

of the film diode; it improves its stability by many orders and over weeks. Stability is maintained even under severe shocks. This is evidence of the fact that the sharp point in this case is not used as the other electrode, as in the case of the MOM point contact diode. The nature of hooking is not the main issue, as long as the oxide layer above the islands is fully penetrated by the sharp tip. However, blunting of the tip will lead to absence of electrical contact, hence zero signal output during X band detection.

Thermal cycling between dry ice and boiling water temperatures has an effect on diode performance in detection. This is most likely due to the nature of mounting of the whisker in a lay-down position. Heating and cooling then cause the stem of the whsiker to expand or contract that result in lateral movement of the bent tip. This is clearly demonstrated in the experiment when the variation in responsivity is repeatable during thermal cycling.

CONCLUSIONS

It is felt that the introduction of the whisker tip has enhanced the responsivity of the film diode over that for interconnected arrays. The sharp tip local field enhancement and island array selection are not significantly degraded with a hooked tip, which improves the stability of the film diode by many orders. The planar nature of the film diode with the film and the whisker in parallel planes renders the diode immune to ambient vibrations. However, the bent tip in the vertical direction (see Fig. 1) tends to move under thermal fluctuations resulting from the thermal expansion and contraction of the stem of the whisker.

It is expected that when a configuration is devised similar to that for the point contact diode [3] , where no lateral movement of the tip is allowed, thermal susceptibility of the film diode will be greatly alleviated. Thickness of the tunneling region is fixed by initial film deposition, which determines inter-island spacing. This feature is extremely desirable for thermal stability; while in the point contact diode, oxide layer penetration depth varies with temperature even with a hooked tip.

Acknowledgements: This work is supported by Office of Naval Research Contract N00014-83-K-0569 and Army Research Office Contract DAAG 29-83-G-0114.

REFERENCES

1. Bor-long Twu, and S. E. Schwarz, Appl. Phys. Lett. 26, 672 (1975).

   S. Okamura, and K. Ejichi, Trans. Inst. Electron. Commun. Eng., Jpn., Sec. E E60, 166 (1977).
2. C. Yu, S. A. Yekranglan and A. W. Frizzell, Conf. Digest 8th International Conference on Infrared and MM Waves, T 6.3 (Miami Beach, Florida, Dec. 12-17, 1983).
3. See previous paper in conference digest.

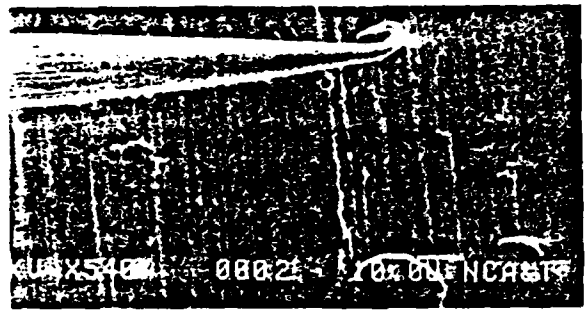

a

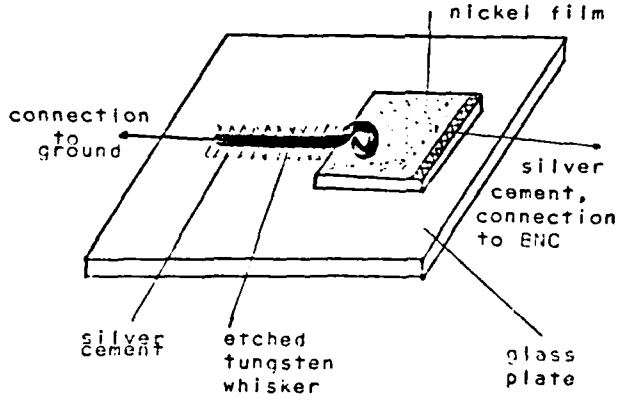

b

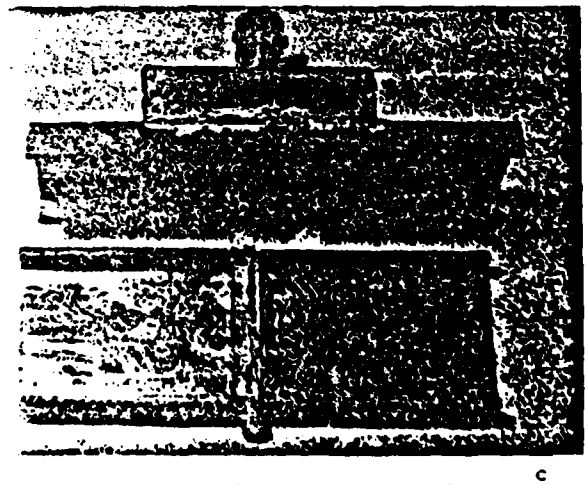

c

Fig. 1. a - optimally hooked tip
b - Sketch of film diode and mount
c - Waveguide diode packaging.

Proceedings of SPIE—The International Society for Optical Engineering

Volume 717

Reliability Considerations in Fiber Optic Applications

Dilip K. Paul
Chair/Editor

Sponsored by
SPIE—The International Society for Optical Engineering

Cooperating Organizations
Center for Applied Optics/University of Alabama in Huntsville
Center for Electro-Optics/University of Dayton
Georgia Institute of Technology
Institute of Optics/University of Rochester
Optical Sciences Center/University of Arizona
Tufts University/Electro-Optics Technology Center

25-26 September 1986
Cambridge, Massachusetts

Published by
SPIE—The International Society for Optical Engineering
P.O. Box 10, Bellingham, Washington 98227-0010 USA
Telephone 206/676-3290 (Pacific Time) • Telex 46-7053

Guided transmission for 10 μm tunable lasers

C. Yu, A. Sabzali, and A. Yekrangian

Electrical Engineering Department, North Carolina A & T State University
Greensboro, NC 27411

Abstract

Mid infrared laser technology centered around 10μm has been driven by the availability of highly efficient, high power tunable CO_2 lasers, continuously tunable lead salt diode lasers, and the rapidly advancing infrared fiber technology. Utilization of such systems is already becoming commonplace in medicine and laser heterodyne spectroscopic systems for remote sensing. These applications are increasingly requiring system flexibility, mobility, hence compaction and integration. To meet these needs, some steps toward 10 μm system integration and compaction have been explored with available mid IR components.

We will report on our studies in the CO_2 laser + metallic piping/fiber + detector system and the tunable diode laser (TDL) + fiber + detector system for heterodyning. Metallic piping will be compatible with w/g CO_2 laser and w/g packaged detectors, where the i.f. beat will be in the microwave region. Fibers will be compatible with TDL for direct butting, but incompatible with w/g packaged detectors. There is also severe thermal gradient between fiber section in the TDL coldhead at LH_2 or LN_2 temperatures, and section at room temperature. Current technology provides lowloss, rugged, near single mode piping, but appreciably higher loss, fragile, chemically unstable multimode fibers. However, there is no doubt fibers will be the ultimate mid IR laser system integration medium, so most of our efforts are in fiber testing and fiber system integration. Comparison studies have been done on relevent fiber parameters, such as loss, toxicity, hygroscopicity, refractive index, flexibility, shelf life, and thermal behavior at low temperatures of crystalline KRS-5, halide and chalcogenide glass fibers. Emphasis is placed on thermal shock evaluation at LN_2 and LH_2 temperatures with respect to mode structure, flexibility and shelf life.

Introduction

Optoelectronic systems operating in the mid and far infrared have found special applications that utilize the unique characteristics of this region of the spectrum. Thus, coherent or heterodyne laser systems have been in use in the field of high resolution spectroscopy in the monitoring of atmospheric and automobile exhaust gaseous pollutants; such systems are also installed as airborne laser scanning systems that require visibility under adverse weather conditions, such as fog, haze, moderate rain, smoke and dust; endoscopic laser treatment and laser surgery delivery systems, to name a few. These major areas of application increasingly call upon high level of system mobility, greatly enhanced mechanical flexibility and adaptability, stability and reliability. Current systems normally incorporate IR transmissive and reflective optics in the form of lenses and mirrors, which are bulky, costly and easily penetrated by environmental factors. These systems lack flexibility, stability, reliability and portability. IR systems must therefore duplicate those in the visible through system integration and compaction.

Portability calls for down scaling of system size through miniturization of the source, detector and the guiding medium simultaneously for component dimensional compatibility. The development of lead salt diode lasers as alternative and complementary sources to CO and CO_2 lasers is an important technological advance in the ultimate integration and compaction of mid and far infrared communication links. Advances in HgCdTe and metal-oxide-metal (MOM) thin film detectors lend high speed to these systems. The broadening market has brought about portable high-power CO and CO_2 lasers. The guiding media of hollow metallic pipes and fibers are maturing at a frantic pace, leading to rapidly decreasing fiber attenuation with anticipated figures in the Rayleigh scattering limit of 0.01 dB/Km. The introduction of such guiding media will eliminate conventional lenses and mirrors and similar accessories, resulting in totally integrated and compacted infrared optoelectronic systems.

The idea of IR system integration and compaction via the fiber guiding medium was conceived by us in the late seventies [1]. However, due to the lack of IR fibers at that time, one of the alternatives was extending the microwave technique by using small, hollow metallic waveguides to gain flexibility. Even at present, such metallic piping is competitive with IR fibers in numerous system characteristics. The room temperature MOM diodes being developed by us has the advantage of the elimination of the dreaded cryogenic environment, that is required by other types of detectors. Such an environment is a significant obstacle to system integration and compaction.

Laser heterodyne system integration schemes at 10.6 μm

A. A completely metallic waveguide link is possible with dimensions compatible with the waveguide CO_2 laser and waveguide packaged MOM discontinuous film or point contact diodes. In the heterodyne scheme, the laser beat frequency will be in the GHz range, and this radiation can be directed through waveguide transitions to standard microwave waveguides.

B. A totally IR fiber link is possible by direct butting of the fiber to the TDL source at one fiber end, with the other end directly butted to a mixer diode, which can be the sputtered MOM discontinuous Ni film chip array [2] on a substrate or the HgCdTe diode. The mixer diode output will then have to be guided by microwave waveguides.

C. A hybrid metallic piping with TDL source system is conceivable, in which the TDL is housed in the metallic waveguide, which is connected with the waveguide packaged mixer diode (MOM) via waveguide transitions. The entire system will be one waveguide package, from which the microwave beat frequency can be tapped directly.

C. Hollow piping studies will concentrate on the fabrication of very small diameter waveguides for ultimate flexibility with guide wall material selection for ultimate low loss. Testing will be conducted with both CO_2 laser and TDL sources.

D. Infrared fiber in-house testing will continue with available fibers on significant fiber parameters such as transparency, attenuation, toxicity, solubility, hygroscopicity, refractive index, mechanical strength, flexibility, thermal behavior, photosensitivity and stability. The temperature range of interest covers from LH_2 to LN_2 to room temperature and above 100° C.

E. MOM film diode research will continue for diode packaging in the infrared with mounting in metallic waveguides, sputtering on substrates and directly sputtering onto fiber end.

F. Specific system experiments will be carried out on CO_2 laser beating in hollow waveguide and IR fiber; CO_2 and TDL beating experiments is of interest. The ultimate packaged system will be tested.

Component Technology Status Review

A. Status of hollow metallic waveguides

Based on the early work on infrared hollow metallic waveguides by E. Garmire [3], M. E. Marhic [4], our work [1] and others, several developers of medical products have reported the development of hollow waveguide CO_2 laser delivery systems [5]. Recently, a surgical laser product that incorporated a 2 mm diameter hollow waveguide arm developed by Laakmann Electro-Optics has been introduced into the market.

The major advantages of such a guiding medium lie in the basic properties of the metallic waveguide, such as preservation of polarization, low metallic losses on guide wall, virtually no upper limit on power to be transmitted, and immunity to adverse environment. These waveguides are dimensionally compatible with mixer packages that are housed in microwave waveguides and CO_2 waveguide lasers.

For these waveguides to be highly flexible, they must be of very small cross sectional dimensions. This normally results in high launch loss unless additional lenses are used for initially beam guiding. Nevertheless, these lenses can be housed in mechanical structures as part of the waveguide package to achieve high level of sturdiness. There is no sacrifice in system size for CO_2 laser sources, but some for TDL sources. Recent results report[5] an aluminum rectangular waveguide of a size of 0.5 mm x 8 mm, having an 83% transmission efficiency, which decreases to about 70% for a 90 degree bend with a 0.1 m radius; to about 50% for a 360 degree bend; to about 60% for a 180 degree twist.

B. Status of mid and far IR fibers

There is no doubt the current surge of activities in the research on IR fibers is the result of prospective application of these fibers in wide areas of medical practice, such as endoscopes and laser delivery system in surgery [6]. These initial requirements on fibers for sufficient flexibility, power carrying capability, resonably low loss and absence of toxicity, chemical inertness are for the purpose of replacing articulated arms and the use of natural body orifices for nonintrusive diagnostics and surgery. These can be satisfied with fibers of mm diameter and losses of fractions of a dB per meter. Current fibers do satisfy these conditions. However, for future pinpoint surgery with highly localized burns, the development of much smaller diameter and even single-mode fibers is essential. Such requirements will then match those in high speed IR communication systems.

Some highly indicative results on fiber loss have been presented in the literature with reference to zirconium fluoride glass, Chalcogenide glass (AsGeSe) and (GeSeSb), metal halide and KRS-5 fibers. Fiber loss falls in the range of 1-20 dB/m for 10.6 μm far infrared fibers and less than 1 dB/m for 2-4 μm mid infrared fibers. ZnSe fiber of 1 mm diameter and 30 cm length was reported to have a 60% transmission at 10 μm [8]. We have been able to obtain only a limited number of fibers of different variety and of less than a foot of useful length. These are early fiber versions from Prof. Katzir of Tel Aviv Univ., Dr. Hartouni of General Dynamics, and Dr. Harrington of Hughes (we understand he is no longer at Hughes), and a Galileo fiber. These sources have supplied us some fiber data, intrinsic to the fibers, and we have tested these fibers under our application conditions. Only qualitative conclusions will be drawn on the performance of these fibers, since no prior discussions have been held with our fiber sources.

Data supplied by the sources and some of our test results are presented in Table 1 below.

Table 1

IR FIBER	SILVER HALIDE (AgCl)	CHALCOGENIDE GLASS (AS3S2)	CHALCOGENIDE GLASS (Ge15AS10Se75)	CHALCOGENIDE GLASS* (Ge28Sb12Se60)
PROPERTY				
TRANSMISSION RANGE(μm)	0.6-20	0.7-10	0.9-15	5-10
LOSSES(dB/m)	1	10-16	10-16	6-8
TOXICITY	NO	NO	NO	NO
SOLUBILITY (g/100)	1.5×10^{-4}	--	--	--
DIAMETER(um)	1000	--	--	300
MODE	MULTIMODE	MULTIMODE	MULTIMODE	MULTIMODE
ABSORPTION COEFFICIENT(cm^{-1})	9×10^{-5}	--	--	--
REFERACTION INDEX	1.98-2	2.39	2.48	2.6
TENSILE STRENGTH(kg/mm^2)	2-25KBAR	GOOD	GOOD	160
HARDNESS	2	--	171	150
FLEXIBILITY	YES	YES	YES	YES
CRYSTAL STRUCTURE	PC	PC	PC	PC
PHOTOSENSITIVITY	NO	NO	NO	NO
TRANSMISSION AT LN2 TEMP.(77 K)	--	75%	75%	--

* COMMERCIAL

These early fibers are generally quite lossy even for less than one foot lengths, possibly due to our crude input coupling. Some fibers were tested in the dark room and some showed aging effect. They were all quite flexible and possessed adequate mechanical strength under 90 degree bending. Fiber loss increased when immersed in LN_2 bath with a 75% drop in transmission from room temperature values. Since these fibers were uncladded,

and multimode, the mode structure observed was complex. A schematic of the fiber testing setup is shown in Fig. 1, and a pictorial view of the actual setup is shown in Fig. 2.

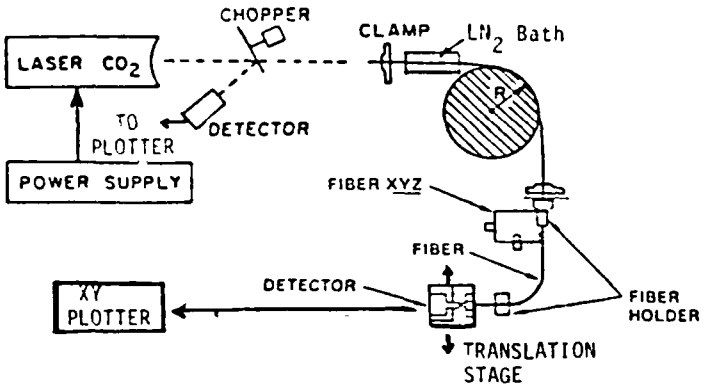

Fig. 1. Schematic of fiber testing setup.

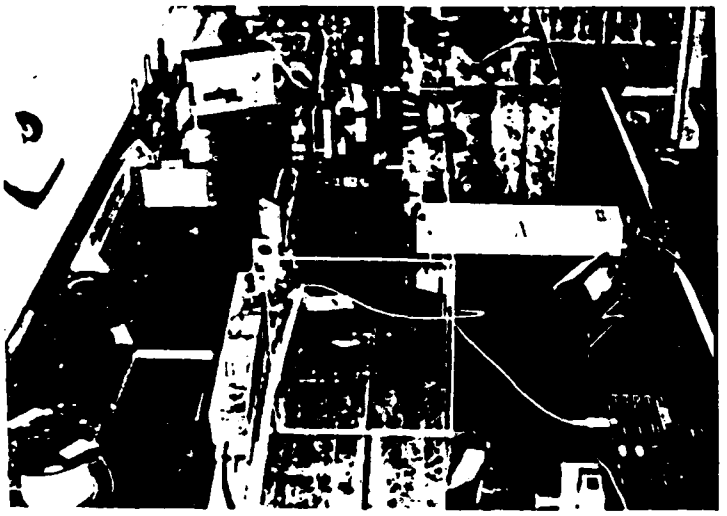

Fig. 2a. Overview of fiber testing setup.
A - HeNe laser;
B - CO_2 laser.

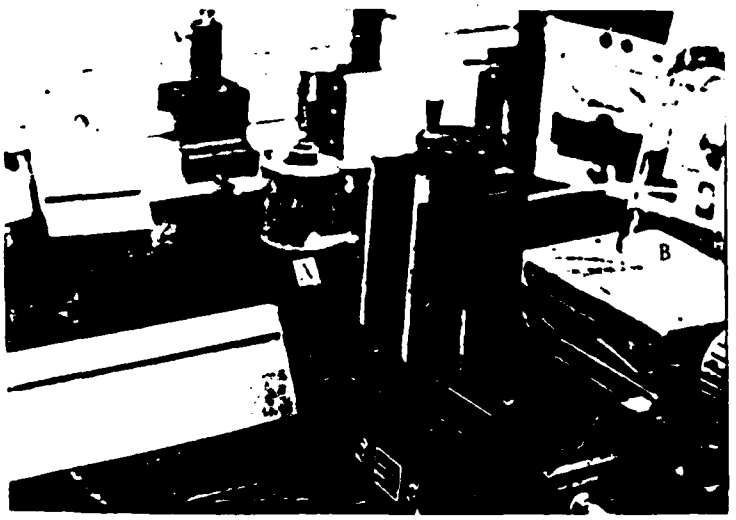

Fig. 2b. Closeup view of setup.
A - fiber input end;
B - bottle serving as variable diameter drum.

Since some fibers were photosensitive, the testing facility was set up in a dark room illuminated by red light only. A Laakmann waveguide CO_2 laser served as the source, and a standard low power HeNe laser was used for fiber alignment. Fiber loss measurement was based on the cut back method. Since the number of fibers we had were few, and fiber length was short, all tests were performed and data gathered before the cut back technique was used. Fibers were tested at LN_2 temperature by immersing them in a LN_2 bath. Fiber loss was measured before and after the immersion for the straight section and with a 90 degree bend. No reduction in fiber flexibility was observed. The bending radius was varied by wrapping the fiber around a cone-shaped glass flask with a narrow neck and a wide base. Its mounting on a vertical jack provided the necessary vertical motion for the flask, and thus a variable wrapping radius for the fiber.

C. Status of Laser Sources

Tunable diode lasers (TDL) are currently the only commercially available semiconductor lasers that lase in the 3-30 μm region. These lead salt TDL's are dimensionally compatible with IR fibers and potential IR communication links, since they are inherently fast devices with rise and fall time in the 100 psec range. However, current diode technology imposes a cryogenic environment for a below 77 K operating temperature. Early TDL's in the late seventies first applied to high resolution laser spectroscopy were plagued by reliability and lifetime problems, as witnessed by one of the authors. The eighties have seen dramatic improvements in device fabrication, packaging and testing that have led to multiyear device lifetimes. The early broad-area homostructure devices are the simplest, and hence most reliable. But poor waveguiding of the planar Fabry Perot cavity leads to excessive loss, and uncontrollable mode structure. The improved mesa stripe geometry raises the operating temperature, and in some cases to as high as 118 K [9]. It also provides a wider tuning range and improved mode structure. The introduction of the heterostructure fabricated by LPE and even MBE leads to quantum well lasers with very thin and uniform epilayers, and hence very low threshold and higher operating temperatures, to as high as 174 K cw and 241 K pulsed.

It is anxiously anticipated that in the near future the severe cryogenic environment of LH_2 or LN_2 can be lifted so that miniature refrigerators can be used for nominal cooling of the high temperature TDL's. This will result in much improved dimensional compatibility of these sources with IR fibers, and thus truly integrated and compacted IR systems.

For completeness, some commercial CO_2 lasers in the market are tabulated in Table 2, with emphasis on small size, power level and tunability. In comparison with TDL's, these sources are grossly larger in size and poorer in portability. This is only a very small sample of the market, and no particular preference is given to any manufacturer.

Table 2

MANUFACTURER	MODEL	SIZE(in)	SIZE OF POWER SUPPLY(in)	POWER	TUNABILITY RANGE
LINE LITE LASER CORP.	945	5.5H X 6W X 24.5L	BUILT IN	7W TYP 5W MIN	9-11.4μm
,,	941S	4H X 5.5W X 19.5L	9H X 9.5W X 12L	3.5W TYP 3W MIN	,,
LASER PHOTONICS	LS-15	3.5H X 3.2W X 13L	3.5H X 8.4W X 14L	1.5W	9.2-10.8 μm
,,	LS-55	3.5H X 3.2W X 17.4L	4H X 6.7W X 12.4L	5.5W	,,
HUGHES AIRCRAFT	3800H -GT	8.2H X 6.25W X 16.5L	NOT AVAILABLE	1W	--
,,	3900H	3.27H X 3.89W X 30.5L	,,	20W	

D. Status of Infrared Detectors

There is a large variety of commercial fast solid state detectors, dominated essentially by HgCdTe [10]. This detector is reported to have a 1-25 μm spectral range, a D* that varies from 10^{9} to 10^{11}, and a rise time in the nsec range. The room temperature version certainly qualifies as a dimensionally compatible component in the integration scheme.

Another category of detectors, called the metal-oxide-metal (MOM) diode detector is the subject of our extensive research efforts. This is inherently a room temperature device with a D* of about 10^{14} and is most attractive in view of its extremely fast response time of the order of 10^{-14} sec, giving it a spectral range from the microwave region to the mid infrared. When used for laser heterodyning, it exhibits an IF bandwidth of over 100 GHz.

We have conducted extensive work in the fabrication and testing of a stable, highly responsive and broadband MOM diode for mm wave and infrared detection and mixing. Two highly stabilized versions have emerged so far [11]. Both versions utilize a deliberately hooked tip of an electrolytically etched tungsten whisker to penetrate either fully or partially the naturally grown oxide layer of a nickel post or islands of the discontinuous film, forming an MOM diode with tunneling as the dominant conduction mechanism. The former is the so called point contact diode, and the latter is the discontinuous film diode. The point contact diode is a single diode, while the latter consists of a large collection of MOM junctions randomly connected electrically when nickel is sputtered onto a substrate and the sputtering process terminated before a continuous nickel film is formed. The discontinuous film is inherently nonuniform, so that there are various groupings or clusters of islands with varying spacings between islands. The grouping with very small island spacing is considered optimum for tunneling, but low in overall resistance. However, such groupings can be selected and electrically connected externally in series to increase diode detection output. On the other hand, if single island grouping produces high resistance, then multi-groupings can be connected in parallel to lower overall diode resistance. This latter arrangement is not preferred due to poor tunneling of the single grouping. The long tungsten whisker also serves as a long wire antenna, and is thus incorporated as such in both diode versions. Proper hooking of the whisker tip is extremely important in terms of the performance and stability of the diodes. This is done by controlling the whisker tip etching process. Figures 3 shows two different etched tips and their subsequent hooking. Figure 4 shows the design of an optimum island grouping, called a "chip", and a series connection of these chips.

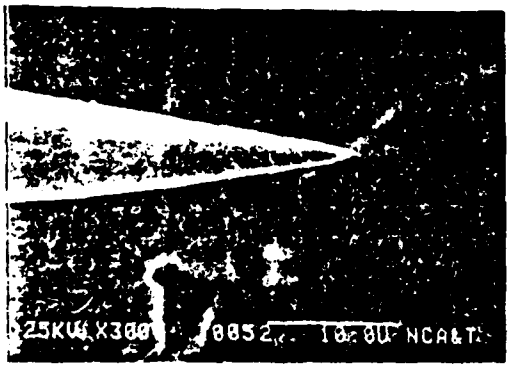

Fig. 3a. Etched tungsten whisker.

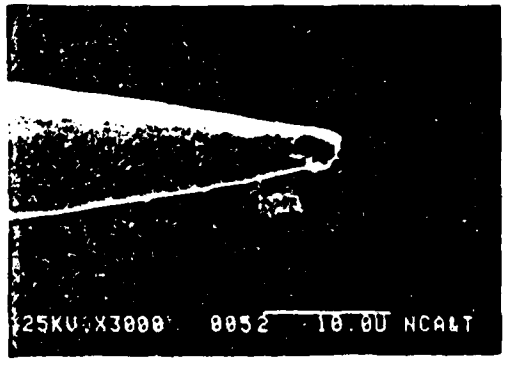

Fig. 3b. Damaged tip when hooked.

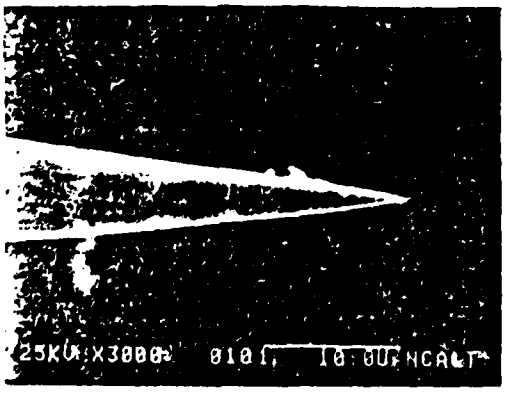

Fig. 3c. Etched tungsten whisker.

Fig. 3d. Optimally hooked tip.

Figure 5 illustrates the assembly of the MOM discontinuous Ni film diode and its packaging in an x band waveguide.

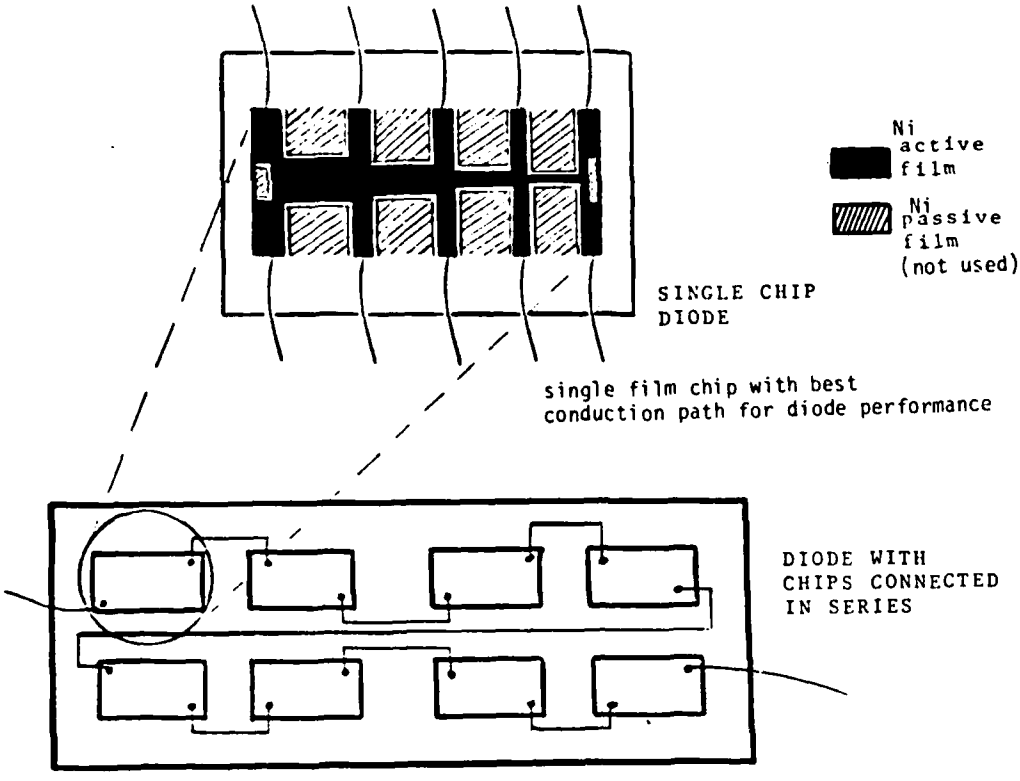

Fig. 4.

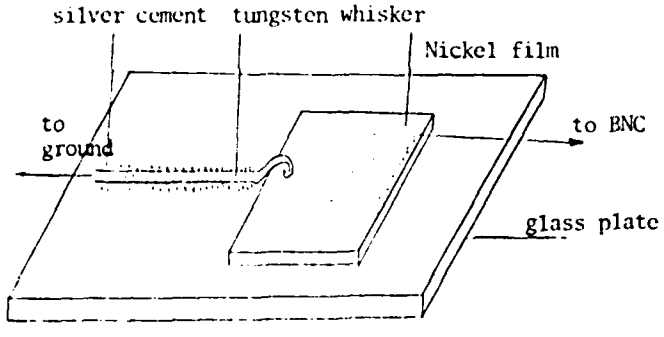

Fig. 5a. MOM discontinuous film diode assembly.

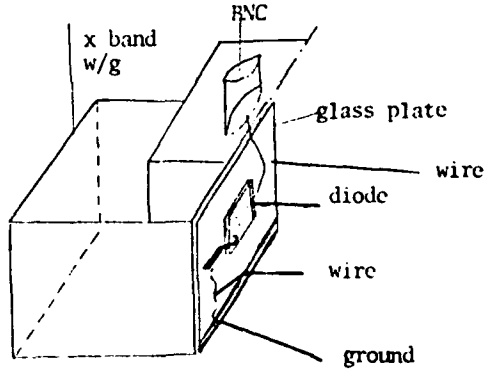

Fig. 5b. Waveguide packaged MOM diode.

Status of Integrated IR Systems

Integrated CO_2 laser systems with hollow piping and fibers have been reported and are in the market in limited numbers. The Laakmann hollow pipe F-75 flexible fiber delivery system is an example with a 75 cm long hollow tube with a 2 mm diameter and an 85% transmission when straight, and a 60% transmission with a 90 degree bend. Obviously this size delivery system cannot provide few-mode or single-mode transmission, highly desirable or even absolutely necessary in IR broadband and coherent communication systems.

We are in the process of fabricating a hollow pipe compatible with rigidly waveguide-packaged lens units for high level of adaptability to TDL front end and HgCdTe or MOM diode receiving end. An illustration of such an arrangement is shown in Fig. 6.

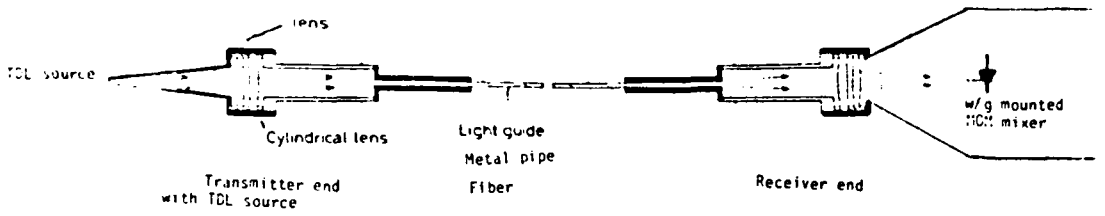

Fig. 6. TDL source + waveguide + detector integrated system package.

The above system is proposed for coupling into hollow pipes of extremely small dimension. Direct butting between TDL and fiber is assumed, unless such butting is not possible in practice. In this case, the above arrangement can also be used for remote TDL to fiber input coupling.

The entirely fiber-and-TDL-and-detector integrated system will be tested and upgraded continuously as improved fibers are becoming available. It is anticipated in a more remote future that TDL can be housed in miniature refrigerators or are free from them completely with high temperature laser diodes.

Acknowledgments

This research work is supported by NASA Research Grant No. NAG 1-407, and Army Research Office Grant No. DAAG29-83-G-0114.

References

1. Yu, C., "Beamshaping and Polarization Control Properties of Flexible Hollow Metallic Rectangular Pipes in the Midinfrared," Proc. IEEE, Vol. 67, pp. 965-966. 1979.
2. Yu, C., and Niczad, A., "Field Enhancement and Increased Island Array Selectivity of Discontinuous MIM Film Diode," Proc. 10th Intern. Conf. on Infrared and MM Waves, pp. 135-136, Orlando, Florida, Dec., 1985.
3. Garmire, E., "Hollow Metal Waveguides with Rectangular Cross Section for High Power Transmission," Proc. SPIE Vol. 484, pp. 112-116, May 1984.
4. Marhic, M. E., "Advances in Infrared Fibers II," Proc. SPIE Vol. 320, pp. 79, 1982.
5. Kubo, U., Hashishin, Y., "Flexible Hollow Metal Lightguide for Medical CO_2 Laser," Proc. SPIE Vol. 494, pp. 79-83, 1984.
6. Fry, S. M., "IR Fibers in Medicine: Applications and Specifications," Proc. SPIE Vol. 618, pp. 40-45, 1986.
7. Hodges, S. E., and Carpenter, J. D., "Spectral Properties of Several Infrared Transmitting Fiber Optics," Proc. SPIE Vol. 618, pp. 32-39, 1986.
8. Pickering, M. A., and Taylor, R. L., "ZeSe Optical Fiber for CO_2 Laser Medical Applications," Proc. SPIE Vol. 576, pp. 16-23, 1985.
9. Wall, D. L., "New Developments in Tunable Diode Laser Sources Relevent to Infrared Fiberoptics Technology," Proc. SPIE Vol. 618, pp. 199-203, 1986.
10. "Solid State Detectors," Photonics Spectra , July Issue, 1985.

END

FEB.

1988

DTIC